Journal of Computational Physics **151,** 534–562 (1999)
Article ID jcph.1999.6195, available online at http://www.idealibrary.com on IDEAL®

Three-Dimensional Stability Analysis of Free Surface Flows: Application to Forward Deformable Roll Coating

M. S. Carvalho[1] and L. E. Scriven

Coating Process Fundamentals Program, Center for Interfacial Engineering and Department of Chemical Engineering and Material Science, University of Minnesota, Minneapolis, Minnesota 55455
E-mail: msc@mec.puc-rio.br

Received September 1, 1998

Coating flows, with a few exceptions, need to be steady and two-dimensional flows. Moreover, the flow states need to be stable at the operating conditions chosen. The goal of stability analysis of coating flows is to determine the region in the parameter space at which the flow is stable and therefore the coated layer uniform. To determine the stability of liquid flows, a generalized eigenvalue problem has to be solved. This paper describes a formulation for a linear, three-dimensional stability analysis of free surface flows that reduces the size of the eigenproblem, decreasing the computational cost, with no further simplification, when compared with the methods reported in the literature. This formulation is used to study the instability that arises in film-splitting flows between counter-rotating rolls in a deformable gap. This flow instability leads to nonuniform coating characterized by a wavy thickness profile in the transverse direction. This patterning is usually referred to as "ribs." This type of instability has received a lot of attention in the literature. However, all previous work has addressed the flow between two rigid rolls. Often, in practice, one of the rolls of a pair is covered by a layer of elastomer. The deformation of the roll cover alters the conformation of the gap, the pressure gradient at the film-split meniscus, and, consequently, the critical parameters at the onset of ribbing change. The results indicate how a deformable cover can be used to delay the onset of ribbing in forward-roll coating.

Key Words: deformable roll coating; linear stability analysis; free boundary problem; Galerkin's method.

[1] Present address: Department of Mechanical Engineering, Pontifícia Universidade Católica do Rio de Janeiro (PUC-Rio), Rua Marques de São Vicente, 225, Gávea, Rio de Janeiro, 22453-900, RJ, Brazil.

0021-9991/99 $30.00

1. INTRODUCTION

Coating a uniform thin liquid layer onto a solid substrate requires a laminar flow, as steady and two-dimensional (except from the edges) as possible. Generally the flow has a free surface, a pair of three-phase static contact "line" regions, and one dynamic one, and it is far from unidirectional. To predict the quality of the liquid layer produced takes accurate theoretical analysis of both steady-state flow and the response of that flow to all the disturbances by which it is tested, including molecular level thermal fluctuations in pressure, velocity, and surface tension that are virtually infinitesimal. The goal is to construct a map of the coating quality as a function of the operating parameters of the process. Such map is often referred to as a *coating window*.

In cases of Newtonian liquids, the governing Navier–Stokes system of the two-dimensional, steady-state viscous flows with free-surfaces can be solved by Galerkin's method with finite element basis functions (Silliman and Scriven [27], Kistler and Scriven [20, 21], Coyle *et al.* [10]). For the stability of the flow with respect to infinitesimal three-dimensional disturbances, the corresponding equations of linear stability theory can also be solved by Galerkin's method and the very same basis functions (Bixler [3], Ruschak [25], Coyle *et al.* [12], Christodoulou and Scriven [8]). The rates of growth of normal modes of disturbances are found by solving a large, generalized, asymmetric matrix eigenvalue problem. A complete solution is not required, for only the eigenvalues with largest real part are needed, i.e., the leading modes. Hence algorithms that deliver all the eigenvalues are prohibitively inefficient. Ruschak [25] and later Coyle *et al.* [12] dodged this inconvenience by neglecting the transient terms in the momentum equations. With this approximation they could reduce considerably the size of the eigenproblem and then compute all the eigenvalue-eigenvector pairs of the reduced problem with a utility program, EISPACK in particular. However, this approximation is valid only at a vanishing Reynolds number or when the marginal stability (onset of instability) of non-periodic disturbances suffices.

This approximation was avoided by Bixler [3] and Christodoulou and Scriven [8]. The latter treated the complete matrix eigenproblem by Arnoldi's method but computed only the leading modes. However, owing to the schemes employed to generate the meshes associated with the basis functions, the infinitesimal disturbances included perturbations of positions of all the finite element nodes, including those interior to the domain. Although these perturbations are consistent with the domain-perturbation formulation of the linear stability theory of free boundary flows it is clear that perturbations of a node located within the domain are not relevant to the stability of the flow. Moreover, the basis overlap ("mass") and weighted-residual sensitivity ("Jacobian") matrices in the method adopted by Christodoulou and Scriven [8] include entries that describe the sensitivity of the solution of the mesh generation equations to the locations of the mesh nodes. Again, it is clear that the stability of the flow cannot depend on the way the mesh used to discretize the flow domain was generated.

In this paper, we show how to avoid the perturbation of interior nodes. The new method reduces the size of the eigenproblem, thereby lowering the cost of computing the needed eigenvalues. It is totally independent of the scheme used to generate a mesh. The new method amounts to returning from domain perturbation to the classical treatment of conditions at free boundaries, that are only infinitesimally displaced from known loci. We use the method to analyze the stability of the flow between a rigid cylinder and a deformable cylinder in counter-rotation, i.e., operating in a forward roll-coating mode.

2. RIBBING INSTABILITY

When a substrate is coated with a thin layer of liquid by the action of rotating rolls, a spreader, brush, or the like, the thickness profile of the layer as coated is wavy in the transverse direction, as sketched in Fig. 1, if the speed of the substrate and applicator is too fast or the liquid viscosity too high. This type of nonuniformity of the flow pattern is commonly called *ribbing*, sometimes *corduroy* or *pin-striping*. It is a result of a flow instability: above a critical value of the dimensionless parameter called the capillary number ($\mu V/\sigma$), the desired two-dimensional flow is unstable and therefore unattainable. The stable state then appears to be a steady, three-dimensional flow whose thickness profile is periodic in the transverse direction.

The instability of the splitting of a liquid layer, or film, as it exits from between rotating rigid rolls or from beneath a spreader has been extensively studied. Using a lubrication approximation, Pearson [22] was the first to analyze why a flow that otherwise leads to a uniform film can turn unstable. He showed that the viscous force destabilizes the film-split meniscus whereas surface tension tends to stabilize it (the proximate destabilizing force is the pressure gradient demanded by the action of viscosity). With that, he recognized that the capillary number, a measure of the ratio of viscous to capillary forces, is the critical parameter in the stability of this class of flows. He could not pinpoint the stability criterion because he did not have available an appropriate boundary condition on Reynolds' equation at the film-split.

Pitts and Greiller [23] developed a stability criterion by considering the pressure gradient near the meniscus of the splitting film in a force balance at the perturbed meniscus (wavenumber of perturbation equal to N), as illustrated in Fig. 2. If the pressure at point **2** is larger than the pressure at point **1**, liquid is driven from **2** to **1**, and the periodic perturbation decays. On the other hand, if the pressure at point **1** is larger, liquid is pushed towards the bulging part of the meniscus and the perturbation grows. The flow is unstable

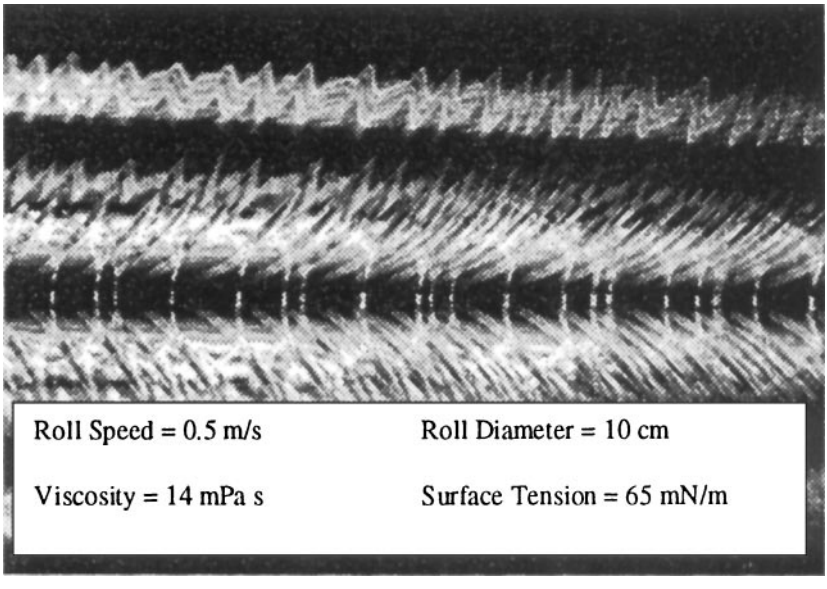

FIG. 1. Ribbing instability in forward film-splitting flows. If the roll speed is too fast or liquid viscosity too high, the coated film is not uniform in the transverse direction.

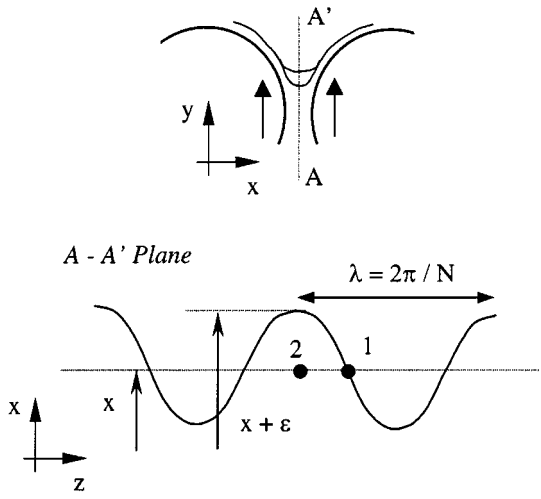

FIG. 2. The film-split meniscus is perturbed in the transverse direction z by a sinusoidal disturbance.

to three-dimensional disturbances. The pressures at points **1** and **2** can be assessed from the curvature of a sinusoidally perturbed meniscus, as shown, and the pressure gradient at the location of the unperturbed meniscus. The perturbed meniscus has a non-vanishing curvature in two orthogonal directions. Thus

$$p_1 = -\frac{1}{Ca}\frac{1}{r(x)} \qquad \text{and} \qquad p_2 = -\frac{1}{Ca}\left(\frac{1}{r(x+\epsilon)} + \epsilon N^2\right) - \frac{dp}{dx}\epsilon.$$

$Ca \equiv \mu V/\sigma$ is the capillary number; $1/r$ is the unperturbed meniscus curvature in the x–y plane; N is the wavenumber of the perturbation; and ϵ is the infinitesimal amplitude of the perturbation. It follows that the flow is stable if

$$\frac{dp}{dx} < \frac{1}{Ca}\left(\frac{1}{r^2}\frac{dr}{dx} + N^2\right).$$

With several further simplifications, Pitts and Greiller [23] estimated that the critical capillary number at onset of ribbing ought to be about

$$Ca = 28\frac{H_0}{R}.$$

Here H_0 is half of the distance between the rolls, and R is the roll radius. This first stability criterion was plainly an estimate.

Savage [31, 32] also employed the lubrication approximation, but used the boundary condition derived by Coyne and Elrod [14] to account roughly for the capillary pressure at the film-split and under the developing film flow downstream of it. The estimate of the pressure gradient at the film-split was more accurate than that of Pitts and Greiller. Savage went on to use linear stability analysis to predict the condition of marginal stability. Fall [16] followed the same approach and examined the time-dependent response to infinitesimal perturbations in order to identify those that grow fastest.

Coyle *et al.* [12] went beyond the lubrication approximation and examined the time-dependent response of the flow between counter-rotating rigid rolls to three-dimensional disturbances by applying linear stability theory to base flows described by the Navier–Stokes system for viscous free-surface flows. They solved for both the base flow and its stability by Galerkin's method and employed finite element basis functions. They found that the earlier stability analyses based on the lubrication approximation underpredicted the capillary number at the onset of ribbing.

All these studies of stability of roll coating flows dealt with flows between two *rigid* rolls. In practice, a pair of rigid rolls is seldom used in forward-roll coating, except sometimes to meter a layer. Usually one of the rolls of each pair of a roll coater is covered with a resilient layer that deforms during operation. The deformation of the roll cover affects the flow rate, meniscus positions, and pressure distribution close to the film-split meniscus. Therefore, it also affects the stability of the flow. Here, the stability of steady film-splitting flows in deformable gaps is analyzed.

3. FILM-SPLITTING FLOWS IN DEFORMABLE GAPS

The flow in a deformable roll coating gap was analyzed by Carvalho and Scriven [5]. Their two-dimensional, steady-state formulation is summarized here. The flow domain and boundary conditions are indicated in Fig. 3. The velocity, pressure, and free surface are governed by the Navier–Stokes system for incompressible fluid and the appropriate boundary conditions:

$$Re\,\mathbf{v}\cdot\nabla\mathbf{v}+\nabla p-\nabla\cdot\boldsymbol{\tau}-St\mathbf{F}=0 \qquad \text{and} \qquad \nabla\cdot\mathbf{v}=0 \quad \text{in } \Omega. \tag{1}$$

The *Reynolds number* $Re\equiv\rho VL/\mu$ characterizes the ratio of inertial to viscous forces. V and L are suitable units of velocity and length, and $\boldsymbol{\tau}\equiv\nabla\mathbf{v}+(\nabla\mathbf{v})^T$ is the viscous stress tensor.

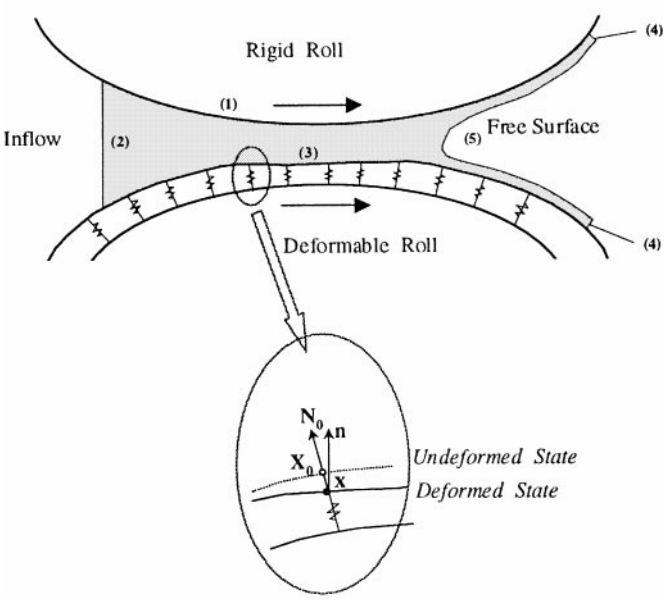

FIG. 3. Sketch of domain for film-splitting flow in a deformable gap. The top roll is rigid; the bottom roll is covered with an elastic layer, modeled here by an array of independent springs.

Because of the presence of a liquid/air interface and a deformable wall, the two-dimensional domain Ω is unknown *a priori* and it is part of the solution.

At the rigid roll surfaces, labeled (1) in Fig. 3, the no-slip and no-penetration conditions take the form

$$\mathbf{v} = \mathbf{V_{Roll}} = W_R R\mathbf{t}. \tag{2a}$$

Here $\mathbf{t}$ is the unit vector tangent to the roll surface, in the direction of rotation; R is the roll radius, and W_R is the angular speed of the rigid roll. Along the inflow boundary ((**2**) in Fig. 3), the inflow condition chosen is a specified constant pressure,

$$p = P_{IN}. \tag{2b}$$

At the deformable roll surface, labeled (**3**) in Fig. 3, the traction exerted by the liquid is balanced by the elastic force on the springs, which is radial,

$$\mathbf{N_0} \cdot (\mathbf{n} \cdot \boldsymbol{\sigma}) = -K\mathbf{N_0} \cdot (\mathbf{x} - \mathbf{X_0}). \tag{2c}$$

$\mathbf{N_0} \cdot (\mathbf{x} - \mathbf{X_0})$ is the normal displacement of the wall; $\mathbf{X_0}$ is the position of a point on the wall in its undeformed state; $\mathbf{N_0}$ is the unit outward normal vector to the undeformed wall at $\mathbf{X_0}$; $\mathbf{n}$ is the unit outward normal vector to the deformed wall at $\mathbf{x}$; $\boldsymbol{\sigma}$ is the Cauchy stress tensor in the liquid; and K is the spring constant, which is related to the roll cover properties in a way described elsewhere (Carvalho and Scriven [7]). At the deformable wall, the liquid neither slips nor penetrates the wall, so that the velocity components in the horizontal direction v_x and vertical direction v_y are

$$v_x = \frac{W_D R}{\mathbf{n} \cdot \mathbf{N_0}} t_x \qquad \text{and} \qquad v_y = \frac{W_D R}{\mathbf{n} \cdot \mathbf{N_0}} t_y. \tag{2d}$$

W_D is the angular speed of the deformable roll. t_x and t_y are the components of the unit vector tangent to the resilient roll surface.

The outflow boundaries (**4**) are located far enough downstream that it seems reasonable to take the flow to be well enough developed that the directional derivative of the velocity in the direction perpendicular to the outlet plane can be set to zero:

$$\frac{\partial \mathbf{v}}{\partial \mathbf{n}} \equiv \mathbf{n} \cdot \nabla \mathbf{v} = 0. \tag{2e}$$

At the free surface (**5**), the traction in the liquid balances the capillary pressure and there is no mass flow across the interface,

$$\mathbf{n} \cdot \boldsymbol{\sigma} = \sigma \frac{d\mathbf{t}}{ds} - \mathbf{n}P_{amb} \qquad \text{and} \qquad \mathbf{n} \cdot \mathbf{v} = 0. \tag{2f}$$

σ is the liquid surface tension.

The dimensionless parameters that govern the base flow are

$$\textit{Reynolds number}, \qquad Re \equiv \frac{\rho \bar{V} H_0}{\mu}$$

$$\textit{Stokes number}, \qquad St \equiv \frac{\rho g H_0^2}{\mu \bar{V}}$$

$$\textit{roll speed ratio}, \qquad S \equiv \frac{W_R}{W_D}$$

$$\textit{dimensionless undeformed clearance (or interference)}, \qquad \frac{H_0}{R}$$

$$\textit{modified elasticity number}, \qquad Ne^* \equiv \frac{\mu \bar{V}}{K R^2}$$

$$\textit{capillary number}, \qquad Ca \equiv \frac{\mu \bar{V}}{\sigma}.$$

Gravitational effects are neglected in the cases analyzed here, i.e., $St = 0$. $\bar{V}$ is the average roll speed. H_0 stands for both the clearance and interference between the undeformed roll surfaces. The first situation is called *positive gaps* and occurs when the center-to-center distance is larger than the sum of the roll radii. If the center-to-center distance is smaller than the sum of the roll radii, the rolls would interfere were they undeformable. Such situations are called *negative gaps*. The modified elasticity number gives a relative magnitude of the roll deformation. The harder the roll cover, the smaller it is; in the limit of rigid rolls, the modified elasticity number is zero.

Elliptic mesh generation was used to map the unknown physical domain Ω into a fixed reference domain Ω_0. Galerkin's method with finite element basis functions was used to solve the system of partial differential equations that describe the problem. Once the field variables were represented in terms of the basis functions, the system of differential equations was reduced to simultaneous algebraic equations for the coefficients of the basis functions of all the fields, i.e., velocity, pressure, and nodal position. This nonlinear set of equations was solved by Newton's method.

4. THREE-DIMENSIONAL LINEAR STABILITY ANALYSIS

The base flow is steady and two-dimensional. The stability of the flow to small disturbances can be judged by solving the time-dependent Navier–Stokes system for the long time behavior of infinitesimal perturbations to the base flow. Because the main goal here is to analyze the onset of ribbing, the perturbations have to be three-dimensional. Because the perturbations are infinitesimal, any possible one can be represented as a linear combination of a complete basis set of linearly independent normal modes, and so it suffices to examine the fate of a generic normal mode. Most convenient in the present case is a set of Fourier modes in the third direction, i.e., transverse to the base flow. The coefficients of these modes are functions of time and the other two dimensions. Accordingly, the disturbed fields, i.e., velocity, pressure, and position of the domain, are written as the sum of the base state and an infinitesimal perturbation ($\Re$ denotes the real part)

$$\begin{aligned} \mathbf{v}(\mathbf{x}, t) &= \mathbf{v_0}(\mathbf{x_0}) + \epsilon \Re\{\mathbf{v}'(\mathbf{x}) \cdot \mathbf{D}(Nz)\, e^{\beta t}\} \\ p(\mathbf{x}, t) &= p_0(\mathbf{x_0}) + \epsilon \Re\{p'(\mathbf{x}) \cos(Nz)\, e^{\beta t}\} \\ \mathbf{x} &= \mathbf{x_0} + \epsilon \Re\{\mathbf{x}' \cdot \mathbf{E}(Nz)\, e^{\beta t}\}. \end{aligned} \tag{3}$$

$\mathbf{v_0}$, p_0, and $\mathbf{x_0}$ are the velocity, pressure, and position of the domain of the base flow, i.e., the two-dimensional, steady-state solution of the free surface flow, which is known a priori. N is the wavenumber in the transverse direction, z ($N = 2\pi/\lambda$, where λ is the wavelength of the perturbation); β is the growth factor. The phase dyadics are

$$\mathbf{D} \equiv (\mathbf{ii} + \mathbf{jj})\cos(Nz) + \mathbf{kk}\sin(Nz) \qquad \text{and} \qquad \mathbf{E} \equiv (\mathbf{ii} + \mathbf{jj})\cos(Nz) + \mathbf{kk}.$$

Their forms are dictated by, respectively, the incompressibility condition and the kinematic relation at the free surface (Bixler [3]).

The velocity $\mathbf{v}$, pressure p, and the position of the domain $\mathbf{x}$ of the disturbed flow are governed by the time-dependent Navier–Stokes system for three-dimensional, free surface flows,

$$Re\left(\frac{\partial \mathbf{v}}{\partial t} + \mathbf{v}\cdot\nabla\mathbf{v}\right) + \nabla p - \nabla\cdot\boldsymbol{\tau} = 0 \qquad \text{and} \qquad \nabla\cdot\mathbf{v} = 0 \quad \text{in } \mathcal{V}^* \tag{4}$$

with the appropriate boundary conditions, i.e., no-slip at solid walls, force balance at the resilient wall, appropriate inflow and outflow boundary conditions, traction balance, and no mass flow across the liquid/air interface. The latter is known as the *kinematic condition*, and, for three-dimensional time-dependent flow, it is written as

$$\mathbf{n}\cdot\frac{\partial \mathbf{x}}{\partial t} - \mathbf{n}\cdot\mathbf{v} = 0 \qquad \text{on } \mathcal{A}^*_{fs}. \tag{5}$$

The force balance at the resilient wall is written as

$$\mathbf{N_0}\cdot(\mathbf{n}\cdot\boldsymbol{\sigma}) = -K\mathbf{N_0}\cdot(\mathbf{x} - \mathbf{X_0}) \qquad \text{on } \mathcal{A}^*_d. \tag{6}$$

The domain of the disturbed three-dimensional flow $\mathcal{V}^*$ is a volume obtained by perturbing the two-dimensional base flow domain (Ω) and extending it over one wavelength in the transverse direction, as indicated in Fig. 4 (cf. Bixler [3]). $\mathcal{A}^*_{fs}$ is the area of the perturbed free surface and $\mathcal{A}^*_d$ is the area of the perturbed deformable roll surface.

The perturbation $\{\mathbf{x}', \mathbf{v}', p'\}$ and its rate of growth β can be found by applying Galerkin's weighted residual method to Eqs. (4)–(6). The weighting functions used for the momentum equation are $\mathbf{D}(Nz)\cdot\boldsymbol{\phi}_i$; and for the continuity equation, $\chi_i\cos(Nz)$. The functions $\boldsymbol{\phi}_i$'s are similar to the vector basis functions used to solve previously for the base flow velocity but now adding the component associated with the transverse direction. The functions χ_i's are the same scalar basis functions used to obtain the pressure field of the base flow. The weighting functions $\overline{\boldsymbol{\phi}_i}$ for the force balance equation at the deformable wall are chosen to be displaced Dirac-delta functions, as it was done for the base flow (see Carvalho and Scriven [5]). The weighted residual equations of momentum, continuity, kinematic condition at the free surface, and force balance at deformable wall are

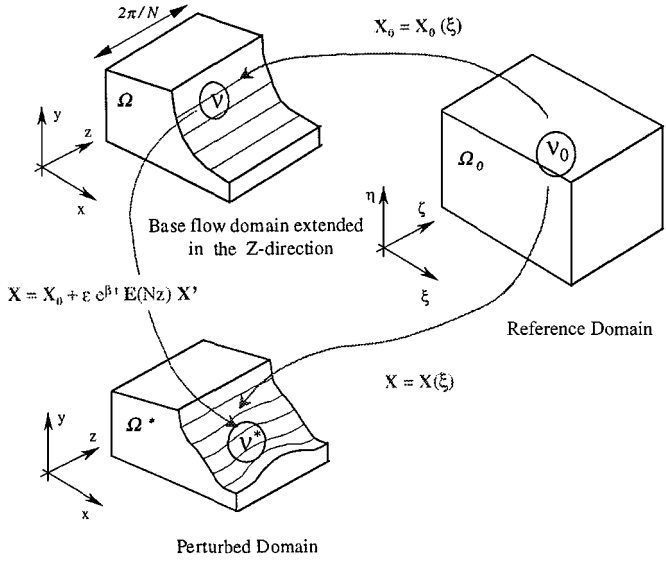

FIG. 4. Diagram of mapping between perturbed three-dimensional domain $\mathcal{V}^*$ and reference domain $\mathcal{V}_0$. The three-dimensional reference domain is obtained by extending the two-dimensional reference domain Ω_0 by one wavelength in the transverse direction.

$$R_i^u = \int_{\mathcal{V}^*} \left\{ \rho\left(\frac{\partial u}{\partial t} + u\frac{\partial u}{\partial x} + v\frac{\partial u}{\partial y} + w\frac{\partial u}{\partial z}\right)\phi_i \cos(Nz) + \left(-p + 2\mu\frac{\partial u}{\partial x}\right)\frac{\partial \phi_i}{\partial x}\cos(Nz) \right.$$
$$+ \mu\left(\frac{\partial u}{\partial y} + \frac{\partial v}{\partial x}\right)\frac{\partial \phi_i}{\partial y}\cos(Nz) - \mu\left(\frac{\partial u}{\partial z} + \frac{\partial w}{\partial x}\right)\phi_i N \sin(Nz)$$
$$\left. - \rho g_x \phi_i \cos(Nz)\right\} d\mathcal{V}^* - \int_{\mathcal{A}^*} [\mathbf{n}\cdot(-p\mathbf{I} + \boldsymbol{\tau})]_x \phi_i \cos(Nz)\, d\mathcal{A}^* \tag{7a}$$

$$R_i^v = \int_{\mathcal{V}^*} \left\{ \rho\left(\frac{\partial v}{\partial t} + u\frac{\partial v}{\partial x} + v\frac{\partial v}{\partial y} + w\frac{\partial v}{\partial z}\right)\phi_i \cos(Nz) + \mu\left(\frac{\partial u}{\partial y} + \frac{\partial v}{\partial x}\right)\frac{\partial \phi_i}{\partial x}\cos(Nz) \right.$$
$$+ \left(-p + 2\mu\frac{\partial v}{\partial y}\right)\frac{\partial \phi_i}{\partial y}\cos(Nz) - \mu\left(\frac{\partial v}{\partial z} + \frac{\partial w}{\partial y}\right)\phi_i N \sin(Nz)$$
$$\left. - \rho g_y \phi_i \cos(Nz)\right\} d\mathcal{V}^* - \int_{\mathcal{A}^*} [\mathbf{n}\cdot(-p\mathbf{I} + \boldsymbol{\tau})]_y \phi_i \cos(Nz)\, d\mathcal{A}^* \tag{7b}$$

$$R_i^w = \int_{\mathcal{V}^*} \left\{ \rho\left(\frac{\partial w}{\partial t} + u\frac{\partial w}{\partial x} + v\frac{\partial w}{\partial y} + w\frac{\partial w}{\partial z}\right)\phi_i \sin(Nz) + \mu\left(\frac{\partial u}{\partial z} + \frac{\partial w}{\partial x}\right)\frac{\partial \phi_i}{\partial x}\sin(Nz) \right.$$
$$+ \mu\left(\frac{\partial v}{\partial z} + \frac{\partial w}{\partial y}\right)\frac{\partial \phi}{\partial y}\sin(Nz) + \left(-p + 2\mu\frac{\partial w}{\partial z}\right)\phi_i N \cos(Nz)$$
$$\left. - \rho g_z \phi_i \sin(Nz)\right\} d\mathcal{V}^* - \int_{\mathcal{A}^*} [\mathbf{n}\cdot(-p\mathbf{I} + \boldsymbol{\tau})]_z \phi_i \sin(Nz)\, d\mathcal{A}^* \tag{7c}$$

$$R_i^c = \int_{\mathcal{V}^*} \left(\frac{\partial u}{\partial x} + \frac{\partial v}{\partial y} + \frac{\partial w}{\partial z}\right)\chi_i \cos(Nz)\, d\mathcal{V}^* \tag{7d}$$

$$R_i^d = \int_{\mathcal{A}_d^*} (\mathbf{N_0} \cdot (\mathbf{n} \cdot \boldsymbol{\sigma}) + K\mathbf{N_0} \cdot (\mathbf{x} - \mathbf{X_0}))\overline{\phi_i} \cos(Nz)\, d\mathcal{A}^* \tag{7e}$$

$$R_i^k = \int_{\mathcal{A}_{fs}^*} \mathbf{n} \cdot (\mathbf{v} - \dot{\mathbf{x}})\phi_i \cos(Nz)\, d\mathcal{A}^*. \tag{7f}$$

$\mathcal{A}^*$ is the area that surrounds the three-dimensional domain. The integrals over $\mathcal{A}^*$ that appear in the momentum weighted residuals can be divided into several parts (see Fig. 4). The contributions from the sides that are x-y planes cancel because the width of the domain is one wavelength. Along solid surfaces, the entire weighted residual is replaced by an essential velocity boundary condition because of the way basis functions are chosen. The only contributions left are the area integrals over the inflow plane, outflow plane, and any perturbed free surfaces that are present. The disturbances are not defined until their behavior on these boundaries is specified. This crucial matter is treated in the next subsection.

To proceed, the perturbed three-dimensional physical domain $\mathcal{V}^*$ is mapped to a known reference three-dimensional domain $\mathcal{V}_0$, as in Fig. 4. The latter is simply obtained by extending the two-dimensional reference domain Ω_0 over one wavelength in the transverse direction. The three-dimensional mapping $\mathbf{x} = \mathbf{x}(\boldsymbol{\xi})$ from $\mathcal{V}_0$ to $\mathcal{V}^*$ is written as a perturbation of the mapping $\mathbf{x_0} = \mathbf{x_0}(\boldsymbol{\xi})$ between the two-dimensional reference domain Ω_0 and the two-dimensional base flow domain Ω, extended over one wavelength in the transverse direction.

The gradient of the perturbed mapping is a kind of deformation gradient:

$$\nabla_{\boldsymbol{\xi}}\mathbf{x} \equiv \mathbf{J} = \begin{pmatrix} \frac{\partial x}{\partial \xi} & \frac{\partial y}{\partial \xi} & \frac{\partial z}{\partial \xi} \\ \frac{\partial x}{\partial \eta} & \frac{\partial y}{\partial \eta} & \frac{\partial z}{\partial \eta} \\ \frac{\partial x}{\partial \zeta} & \frac{\partial y}{\partial \zeta} & \frac{\partial z}{\partial \zeta} \end{pmatrix} = \begin{pmatrix} \frac{\partial x}{\partial \xi} & \frac{\partial y}{\partial \xi} & 0 \\ \frac{\partial x}{\partial \eta} & \frac{\partial y}{\partial \eta} & 0 \\ \frac{\partial x}{\partial \zeta} & \frac{\partial y}{\partial \zeta} & 1 \end{pmatrix}.$$

The Jacobian of this transformation is

$$|\mathbf{J}| = \frac{\partial x}{\partial \xi}\frac{\partial y}{\partial \eta} - \frac{\partial x}{\partial \eta}\frac{\partial y}{\partial \xi} = |\mathbf{J_0}|\left\{1 + \epsilon e^{\beta t}\cos(Nz)\left(\frac{\partial x'}{\partial x_0} + \frac{\partial y'}{\partial y_0}\right)\right\},$$

where $|\mathbf{J_0}|$ is the Jacobian of the two-dimensional mapping from the reference domain Ω_0 to the domain of the base flow Ω. From this it follows that

$$d\mathcal{V}^* = d\Omega\, dz\left\{1 + \epsilon e^{\beta t}\cos(Nz)\left(\frac{\partial x'}{\partial x_0} + \frac{\partial y'}{\partial y_0}\right)\right\}.$$

Thus volume integrals over the perturbed domain $\mathcal{V}^*$ reduce to an area integral over the unperturbed two-dimensional domain Ω and a line integral along the transverse direction z. The volume integrals of Eqs. (7a) to (7d) have the form

$$\int_{\mathcal{V}^*} F(\mathbf{x}, \mathbf{v})\, d\mathcal{V}^*$$

and can be rewritten in the more useful form

$$\int_{\mathcal{V}^*} F(\mathbf{x}, \mathbf{v})\, d\mathcal{V}^* = \int_0^{\frac{2\pi}{N}} \int_\Omega F(\mathbf{x}, \mathbf{v})\, d\Omega\, dz + \epsilon e^{\beta t} \int_0^{\frac{2\pi}{N}} \int_\Omega F(\mathbf{x}, \mathbf{v}) \cos(Nz)\left(\frac{\partial x'}{\partial x_0} + \frac{\partial y'}{\partial y_0}\right) d\Omega\, dz. \tag{8}$$

Now, substituting the disturbed fields (3) into the weighted residual equations (7), linearizing all the terms, and discarding terms of second and higher powers of ϵ yields the so-called weak form of the linear stability problem, i.e., the Galerkin weighted residuals of the equations that govern an infinitesimal perturbation.

The linearization of the derivatives of the perturbed fields with respect to the positions of the perturbed domain follows the general form shown in the example below,

$$\frac{\partial u}{\partial x} = \frac{\partial u_0}{\partial x_0} + \epsilon e^{\beta t}\cos(Nz)\left\{\frac{\partial u'}{\partial x_0} - \frac{\partial u_0}{\partial x_0}\left(\frac{\partial x'}{\partial x_0} + \frac{\partial y'}{\partial y_0}\right) + \frac{|\mathbf{J}'|}{|\mathbf{J}|}\frac{\partial u_0}{\partial x'}\right\},$$

where

$$|\mathbf{J}'|\frac{\partial}{\partial x'} = \frac{\partial y'}{\partial \eta}\frac{\partial}{\partial \xi} - \frac{\partial y'}{\partial \xi}\frac{\partial}{\partial \eta}.$$

For example, the Galerkin weighted residual of the x-component of the momentum equation of the perturbed flow becomes

$$\begin{aligned}
R_i^u = \int_0^{2\pi/N} \cos(Nz)\,dz \Bigg\{ \int_\Omega \Bigg\{ & \rho\left(u_0\frac{\partial u_0}{\partial x_0} + v_0\frac{\partial u_0}{\partial y_0}\right)\phi_i + \left(-p_0 + 2\mu\frac{\partial u_0}{\partial x_0}\right)\frac{\partial \phi_i}{\partial x_0} \\
& + \mu\left(\frac{\partial u_0}{\partial y_0} + \frac{\partial v_0}{\partial x_0}\right)\frac{\partial \phi_i}{\partial y_0} - \rho g_x \phi_i \Bigg\} d\Omega \Bigg\} + \epsilon e^{\beta t}\frac{\pi}{N}\Bigg\{ \beta \int_\Omega \rho u' \phi_i \, d\Omega \\
& + \int_\Omega \Bigg\{ \rho\left[u_0\frac{\partial u'}{\partial x_0} + v_0\frac{\partial u'}{\partial y_0} + u'\frac{\partial u_0}{\partial x_0} + v'\frac{\partial u_0}{\partial y_0}\right]\phi_i + \left(-p' + 2\mu\frac{\partial u'}{\partial x_0}\right)\frac{\partial \phi_i}{\partial x_0} \\
& + \mu\left(\frac{\partial u'}{\partial y_0} + \frac{\partial v'}{\partial x_0}\right)\frac{\partial \phi_i}{\partial y_0} + N^2\mu u'\phi_i - N^2\mu\left(y'\frac{\partial u_0}{\partial y_0} + x'\frac{\partial u_0}{\partial x_0}\right)\phi_i - N\mu\phi_i\frac{\partial w'}{\partial x_0}\Bigg\} d\Omega \\
& + \int_\Omega \Bigg\{ -2\mu\frac{\partial u_0}{\partial x_0}\frac{\partial \phi_i}{\partial x_0} - \mu\left(\frac{\partial u_0}{\partial y_0} + \frac{\partial v_0}{\partial x_0}\right)\frac{\partial \phi_i}{\partial y_0} - \rho g_x \phi_i \Bigg\}\left(\frac{\partial x'}{\partial x_0} + \frac{\partial y'}{\partial y_0}\right) d\Omega \\
& + \int_\Omega \Bigg\{ \rho\left(u_0\frac{\partial u_0}{\partial x'} + v_0\frac{\partial u_0}{\partial y'}\right)\phi_i + 2\mu\frac{\partial u_0}{\partial x'}\frac{\partial \phi_i}{\partial x_0} + \left(-p_0 + 2\mu\frac{\partial u_0}{\partial x_0}\right)\frac{\partial \phi_i}{\partial x'} \\
& + \mu\left(\frac{\partial u_0}{\partial y_0} + \frac{\partial v_0}{\partial x_0}\right)\frac{\partial \phi_i}{\partial y'} + \mu\left(\frac{\partial u_0}{\partial y'} + \frac{\partial v_0}{\partial x'}\right)\frac{\partial \phi_i}{\partial y_0}\Bigg\}\frac{|\mathbf{J}'|}{|\mathbf{J}|}\, d\Omega \Bigg\}.
\end{aligned}$$

The line integrals related with the boundary conditions at inflow, outflow planes and free surfaces were omitted. These terms are treated in the next subsection.

The contribution in the first curly bracket is independent of ϵ and is identically zero: it is exactly the x-component of the momentum weighted residual of the base flow. The factor π/N that multiplies the term proportional to the perturbation parameter ϵ comes from the integral along the transverse direction z of $\sin^2(Nz)$ and $\cos^2(Nz)$. That factor together with $\epsilon e^{\beta t}$ are common to the remaining contributions and can be cancelled because the residual should ultimately vanish in Galerkin's method. What is left is the Galerkin's weighted residual equation for the x-component of the momentum weighted residual of the perturbation flow.

In a similar way, to evaluate the residual equations of the force balance at the deformable wall and the kinematic condition at the free surface, the area integrals over these perturbed

surfaces, $\mathcal{A}_d^*$ and $\mathcal{A}_{fs}^*$, have to be rewritten as integrals over the unperturbed and known deformable wall and free surface areas. They are both extension over one wavelength in the transverse direction of the lines Γ_d and Γ_{fs} that define the position of the resilient wall and free surface of the two-dimensional base flow,

$$\int_{\mathcal{A}_{fs}^*} F(\mathbf{x},\mathbf{v})\, d\mathcal{A}^* = \int_0^{\frac{2\pi}{N}} \int_{\Gamma_{fs}} F(\mathbf{x},\mathbf{v})\, d\Gamma\, dz + \epsilon e^{\beta t} \int_0^{\frac{2\pi}{N}} \int_{\Gamma_{fs}} F(\mathbf{x},\mathbf{v}) \times \left[\cos(Nz)\left(\frac{\partial x_0}{\partial \Gamma} + \frac{\partial x'}{\partial \Gamma} + \frac{\partial y_0}{\partial \Gamma} + \frac{\partial y'}{\partial \Gamma} \right) + N \sin(Nz)\left(x' \frac{\partial x_0}{\partial \Gamma} + y' \frac{\partial y_0}{\partial \Gamma} \right) \right] d\Gamma\, dz \quad (9a)$$

$$\int_{\mathcal{A}_d^*} F(\mathbf{x},\mathbf{v})\, d\mathcal{A}^* = \int_0^{\frac{2\pi}{N}} \int_{\Gamma_d} F(\mathbf{x},\mathbf{v})\, d\Gamma\, dz + \epsilon e^{\beta t} \int_0^{\frac{2\pi}{N}} \int_{\Gamma_d} F(\mathbf{x},\mathbf{v}) \times \left[\cos(Nz)\left(\frac{\partial x_0}{\partial \Gamma} + \frac{\partial x'}{\partial \Gamma} + \frac{\partial y_0}{\partial \Gamma} + \frac{\partial y'}{\partial \Gamma} \right) + N \sin(Nz)\left(x' \frac{\partial x_0}{\partial \Gamma} + y' \frac{\partial y_0}{\partial \Gamma} \right) \right] d\Gamma\, dz. \quad (9b)$$

After substituting the disturbed fields (3) into the weighted residual equation (7e)–(7f), linearizing the terms, and discarding the terms of second and higher orders of ϵ, what is left is the weak form of the linearized kinematic condition and force balance. For example, the Galerkin weighted residual of the kinematic condition of the perturbed flow becomes

$$R_i^k = \int_0^{2\pi/N} \cos(Nz)\, dz \left\{ \int_{\Gamma_{fs}} (\mathbf{n}_0 \cdot \mathbf{v}_0)\phi_i\, d\Gamma \right\} + \epsilon e^{\beta t} \frac{\pi}{N} \left\{ -\beta \int_{\Gamma_{fs}} (x' n_{0x} + y' n_{0y})\phi_i\, d\Gamma + \int_{\Gamma_{fs}} (n_{0x} u' + n_{0y} v' + n_x' u_o + n_y' v_o)\phi_i\, d\Gamma \right\}.$$

Like the momentum residual, the contribution of the first term is independent of ϵ and is identically zero: it is the residual equation of the kinematic condition of the base flow. n_{0x} and n_{0y} are the x- and y-components of the unit vector normal to the unperturbed surface, and n_x' and n_y' are related with the perturbation of the normal vector; they are given by

$$n_x' = \pm \frac{\partial y'/\partial \Gamma_0}{\left[(\partial x_0/\partial \Gamma_0)^2 + (\partial y_0/\partial \Gamma_0)^2 \right]^{1/2}} \quad \text{and} \quad n_y' = \mp \frac{\partial x'/\partial \Gamma_0}{\left[(\partial x_0/\partial \Gamma_0)^2 + (\partial y_0/\partial \Gamma_0)^2 \right]^{1/2}}.$$

Γ_0 stands for the reference domain coordinate along the free boundary.

4.1. Boundary Conditions for the Momentum Equation

As mentioned before, the relevant parts of the area integral over $\mathcal{A}^*$ that comes from the weak formulation of the three-dimensional, time dependent Navier–Stokes equation are the integral over the inflow plane $\mathcal{A}_{in}^*$, outflow plane $\mathcal{A}_{out}^*$, and any free surface $\mathcal{A}_{fs}^*$ that are present:

$$\int_{\mathcal{A}^*} [\mathbf{n} \cdot (-p\mathbf{I} + \boldsymbol{\tau})] \cdot (\mathbf{D}(Nz) \cdot \phi_i)\, d\mathcal{A}^* = \int_{\mathcal{A}_{in}^*} [\mathbf{n} \cdot (-p\mathbf{I} + \boldsymbol{\tau})] \cdot (\mathbf{D}(Nz) \cdot \phi_i)\, d\mathcal{A}^* + \int_{\mathcal{A}_{out}^*} [\mathbf{n} \cdot (-p\mathbf{I} + \boldsymbol{\tau})] \cdot (\mathbf{D}(Nz) \cdot \phi_i)\, d\mathcal{A}^* + \int_{\mathcal{A}_{fs}^*} [\mathbf{n} \cdot (-p\mathbf{I} + \boldsymbol{\tau})] \cdot (\mathbf{D}(Nz) \cdot \phi_i)\, d\mathcal{A}^*.$$

The disturbance of the flow is only defined after its behavior at the boundaries is specified. Unlike the free surface $\mathcal{A}^*_{fs}$, the positions of the inflow and outflow planes of the disturbed flow are fixed. At the free surfaces, the normal component of the traction must be balanced by capillary pressure and the tangential component, or shear stress, must vanish,

$$[\mathbf{n} \cdot (-p\mathbf{I} + \boldsymbol{\tau})] = \sigma(\nabla \cdot \mathbf{n})\mathbf{n} - \mathbf{n}P_{amb}.$$

This is a three-dimensional version of the boundary condition (2f) used for the base flow.

The order of the derivatives in the area integral over the free-surface can be reduced with the surface divergence theorem,

$$\int_{\mathcal{A}^*_{fs}} [\mathbf{n} \cdot (-p\mathbf{I} + \boldsymbol{\tau})] \cdot (\mathbf{D}(Nz) \cdot \phi_i)\, d\mathcal{A}^* = \oint \sigma \mathbf{m} \cdot (\mathbf{D}(Nz) \cdot \phi_i)\, dl$$
$$- \int_{\mathcal{A}^*_{fs}} \sigma \nabla_{II} \cdot (\mathbf{D}(Nz) \cdot \phi_i)\, d\mathcal{A}^* - \int_{\mathcal{A}^*_{fs}} P_{amb}\mathbf{n} \cdot (\mathbf{D}(Nz) \cdot \phi_i)\, d\mathcal{A}^*.$$

$\mathbf{m}$ is the binormal vector along the surface boundary curve and $\nabla_{II}\cdot$ is the surface divergence operator, viz. $\nabla - \mathbf{nn} \cdot \nabla$. The integrals over the perturbed free surface area $\mathcal{A}^*_{fs}$ can be rewritten following Eq. (9a).

The boundary conditions along the inflow and outflow plane used for the three-dimensional perturbed flow were simply an extension of the conditions used for the two-dimensional base flow. At the inflow, the pressure was taken to be constant, therefore

$$p' = 0.$$

At the outflow plane, the directional derivative of the perturbed velocity in the direction perpendicular to the outflow plane was set to zero:

$$\mathbf{n_0} \cdot \nabla \mathbf{u}' = 0.$$

4.2. Restriction of Domain Perturbation to Free Surfaces

As noted in the Introduction, earlier analyses have followed the prescription of domain perturbation and displaced the nodes associated with finite element basis functions. For linear stability analysis this is quite unnecessary. If the domain perturbation approach is retained, only the positions of nodes on free surfaces (or other free boundaries) need to be perturbed as part of a generic disturbance. This is done here, by setting the domain perturbation to

$$\mathbf{x}' = H^{(0)}(\mathbf{x_0})h'\mathbf{n}, \qquad H^{(0)} = \lim_{\delta \to 0} H^{(\delta)}, \tag{10}$$

where $H^{(\delta)}$ is a smooth function defined by

$$H^{(\delta)}(\mathbf{x_0}) = \begin{cases} 1, & \text{if } \mathbf{x_0} \in \Gamma; \\ 0, & \text{if } \mathbf{x_0} \in \Omega \text{ and } |\mathbf{x_0} - \mathbf{x_b}| > |\delta\mathbf{n}|, \forall \mathbf{x_b} \in \Gamma; \\ \text{smooth function}, & \text{if } \mathbf{x_0} \in \Omega \text{ and } |\mathbf{x_0} - \mathbf{x_b}| < |\delta\mathbf{n}|, \forall \mathbf{x_b} \in \Gamma. \end{cases}$$

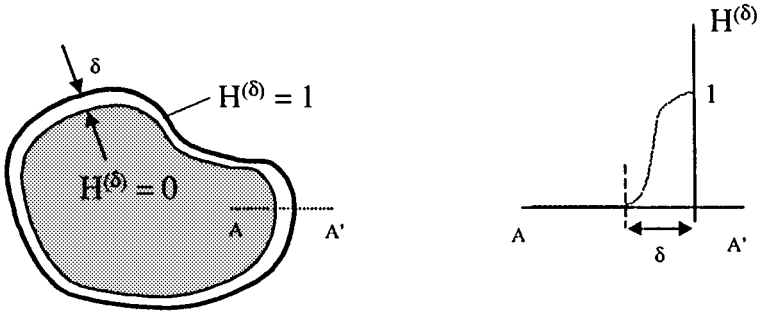

FIG. 5. Function $H^{(\delta)}(\mathbf{x_0})$ used to define the domain of the perturbation. It vanishes inside the domain, it is equal to one at the boundaries, and close to the boundaries, it smoothly decays from 1 to 0.

It vanishes inside the domain, it is equal to one at the boundaries and close to the boundaries (inside a ring of thickness δ), and it smoothly decays from 1 to 0, as sketched in Fig. 5. h' is a scalar function that gives the amplitude of the perturbation, and $\mathbf{n}$ is the unit normal vector to the unperturbed domain boundary; see Fig. 6. The amplitude of the boundary displacement h' differs from zero only where the domain perturbation is relevant, viz. free-surfaces and other free boundaries, like a deformable wall. In finite element representation it is a linear combination of basis functions ϕ_i on the boundary of the base flow domain,

$$h'(\mathbf{x_{fs}}) = \sum_{i=1}^{L} H'_i \phi_i(\mathbf{x_{fs}}).$$

In this way, the number of basis function coefficients ("degrees of freedom") associated with the disturbance of the domain is reduced to one per node located on free-surfaces (or other free boundaries).

The definition of the domain perturbation in (10) also simplifies the weighted residual equations substantially because of two properties of the function $H^{(0)}$,

$$\int_\Omega F(\mathbf{x_0})\left(\frac{\partial H^{(0)}}{\partial x_0} + \frac{\partial H^{(0)}}{\partial y_0}\right) d\Omega = \int_\Gamma F(\mathbf{x_0})\, d\Gamma \qquad \text{and} \qquad \int_\Omega F(\mathbf{x_0}) H^{(0)}\, d\Omega = 0.$$

These allow terms of the weighted residual equations which have derivatives of node

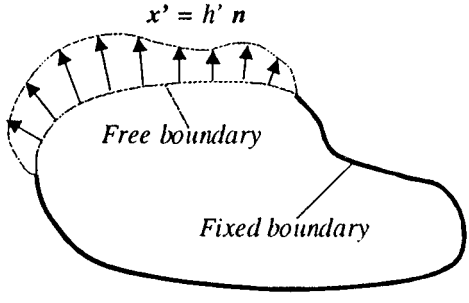

FIG. 6. The perturbation of the free surface is restricted to displacements along the normal direction. The amplitude is given by a scalar function h'.

displacement to be simplified to line integrals; in general form,

$$\int_\Omega F(\mathbf{x_0})\left(\frac{\partial x'}{\partial x_0}+\frac{\partial y'}{\partial y_0}\right)d\Omega=\int_\Gamma h'F(\mathbf{x_0})\,d\Gamma$$

$$\int_\Omega F(\mathbf{x_0})\frac{\partial(*)}{\partial x'}\frac{|\mathbf{J}'|}{|\mathbf{J}|}\,d\Omega=\int_\Gamma h'F(\mathbf{x_0})\frac{\partial x_0}{\partial\Gamma}\frac{\partial(*)}{\partial\Gamma}\,d\Gamma$$

$$\int_\Omega F(\mathbf{x_0})\frac{\partial(*)}{\partial y'}\frac{|\mathbf{J}'|}{|\mathbf{J}|}\,d\Omega=\int_\Gamma h'F(\mathbf{x_0})\frac{\partial y_0}{\partial\Gamma}\frac{\partial(*)}{\partial\Gamma}\,d\Gamma.$$

$d\Gamma$ is the differential along the portion of the boundaries of Ω where h' differs from zero.

For example, the x-component of the perturbed momentum weighted residual after removing the steady state contribution, that is identically zero, cancelling the term $\epsilon e^{\beta t}\pi/N$, and after all integrals simplifications is

$$\begin{aligned}R_i^u=\beta\int_\Omega\rho u'\phi_i\,d\Omega+\int_\Omega\Bigg\{&\rho\left[u_0\frac{\partial u'}{\partial x_0}+v_0\frac{\partial u'}{\partial y_0}+u'\frac{\partial u_0}{\partial x_0}+v'\frac{\partial u_0}{\partial y_0}\right]\phi_i\\&+\left(-p'+2\mu\frac{\partial u'}{\partial x_0}\right)\frac{\partial\phi_i}{\partial x_0}+\mu\left(\frac{\partial u'}{\partial y_0}+\frac{\partial v'}{\partial x_0}\right)\frac{\partial\phi_i}{\partial y_0}+N^2\mu u'\phi_i-N\mu\phi_i\frac{\partial w'}{\partial x_0}\Bigg\}d\Omega\\+\int_\Gamma\Bigg\{&-2\mu\frac{\partial u_0}{\partial x_0}\frac{\partial\phi_i}{\partial x_0}-\mu\left(\frac{\partial u_0}{\partial y_0}+\frac{\partial v_0}{\partial x_0}\right)\frac{\partial\phi_i}{\partial y_0}-\rho g_x\phi_i\\&+\rho\left(u_0\frac{\partial u_0}{\partial\Gamma}\frac{\partial x_0}{\partial\Gamma}+v_0\frac{\partial u_0}{\partial\Gamma}\frac{\partial y_0}{\partial\Gamma}\right)\phi_i+2\mu\frac{\partial u_0}{\partial\Gamma}\frac{\partial x_0}{\partial\Gamma}\frac{\partial\phi_i}{\partial x_0}+\left(-p_0+2\mu\frac{\partial u_0}{\partial x_0}\right)\frac{\partial x_0}{\partial\Gamma}\frac{\partial\phi_i}{\partial\Gamma}\\&+\mu\left(\frac{\partial u_0}{\partial y_0}+\frac{\partial v_0}{\partial x_0}\right)\frac{\partial y_0}{\partial\Gamma}\frac{\partial\phi_i}{\partial\Gamma}+\mu\left(\frac{\partial u_0}{\partial\Gamma}\frac{\partial y_0}{\partial\Gamma}+\frac{\partial v_0}{\partial\Gamma}\frac{\partial x_0}{\partial\Gamma}\right)\frac{\partial\phi_i}{\partial y_0}\Bigg\}h'\,d\Gamma.\end{aligned}\tag{11}$$

The line integrals corresponding to the boundary conditions at the inlet plane, outlet plane, and free surface were not included in the expression above.

In matrix vector form, the set of algebraic equations that governs the generic perturbation is

$$\mathbf{R}(\mathbf{c}')=0,$$

where $\mathbf{R}$ is the column vector of weighted residual equations and $\mathbf{c}'$ is the column vector of coefficients of the finite element basis functions with which the perturbation of velocity, pressure, and free boundaries position are represented.

When this set of equations is expanded in Taylor series and truncated at order $O(\mathbf{c}'^2)$ on the grounds that the perturbation is infinitesimal, the result is the equation set

$$\frac{\partial\mathbf{R}}{\partial\mathbf{c}'}\mathbf{c}'=0.$$

$\partial\mathbf{R}/\partial\mathbf{c}'$ is the matrix of sensitivities of the weighted residuals with respect to the unknown coefficients of the perturbation. It is clear from Eq. (11) that this matrix can be separated into two matrices:

$$\frac{\partial\mathbf{R}}{\partial\mathbf{c}'}=-\beta\mathbf{M}+\mathbf{J}.$$

M is called the mass matrix (actually it represents the overlap of basis functions) and **J** the Jacobian matrix. For free surface flows, both matrices are asymmetric. Moreover, in the class of problems analyzed here, the mass matrix **M** is singular, because the continuity equation and essential boundary conditions do not contain time derivatives.

It follows that the generic perturbation is governed by the generalized, nonsymmetric, and large eigenproblem:

$$\mathbf{J}\mathbf{c}' = \beta \mathbf{M}\mathbf{c}' \tag{12}$$

All entries of the Jacobian and mass matrix including the appropriate boundary conditions for the flow in a deformable roll coating gap are recorded in Table I.

TABLE I

Mass and Jacobian Matrices Entries for Stability of a Deformable Roll Film-Splitting Flow

$$\partial \boldsymbol{R}_i / \partial \boldsymbol{c}'_j = -\beta \boldsymbol{M}_{i,j} + \boldsymbol{J}_{i,j}$$

(I) x-Component of Momentum Equation

$$M_{u'_i,u'_j} = -\int_\Omega \rho \phi_i \phi_j \, d\Omega$$

$$J_{u'_i,u'_j} = \int_\Omega \left\{ \rho \left(u_0 \frac{\partial \phi_j}{\partial x_0} + v_0 \frac{\partial \phi_j}{\partial y_0} + \frac{\partial u_0}{\partial x_0} \phi_j \right) \phi_i + 2\mu \frac{\partial \phi_j}{\partial x_0} \frac{\partial \phi_i}{\partial x_0} + \mu \frac{\partial \phi_j}{\partial y_0} \frac{\partial \phi_i}{\partial y_0} + N^2 \mu \phi_i \phi_j \right\} d\Omega$$

$$- \int_{\Gamma_{in}} \left\{ 2 \frac{\partial \phi_j}{\partial x_0} \phi_i n_{0x} + \frac{\partial \phi_j}{\partial y_0} \phi_i n_{0y} \right\} d\Gamma - \int_{\Gamma_{out}} \frac{\partial \phi_j}{\partial x_0} \phi_i n_{0x} \, d\Gamma$$

$$J_{u'_i,v'_j} = \int_\Omega \left\{ \rho \frac{\partial u_0}{\partial y_0} \phi_j \phi_i + \mu \frac{\partial \phi_j}{\partial x_0} \frac{\partial \phi_i}{\partial y_0} \right\} d\Omega - \int_{\Gamma_{in}} \frac{\partial \phi_j}{\partial x_0} \phi_i n_{0y} \, d\Gamma - \int_{\Gamma_{out}} \frac{\partial \phi_j}{\partial y_0} \phi_i n_{0y} \, d\Gamma$$

$$J_{u'_i,w'_j} = -\int_\Omega N \mu \frac{\partial \phi_j}{\partial x_0} \phi_i \, d\Omega$$

$$J_{u'_i,p'_j} = \int_\Omega \frac{\partial \phi_i}{\partial x_0} \chi_j \, d\Omega + \int_{\Gamma_{out}} \chi_j \phi_i n_{0x} \, d\Gamma$$

$$J_{u'_i,h'_j} = -\int_{\Gamma_{fs}} \left\{ -2\mu \frac{\partial u_0}{\partial x_0} \frac{\partial \phi_i}{\partial x_0} - \mu \left(\frac{\partial u_0}{\partial y_0} + \frac{\partial v_0}{\partial x_0} \right) \frac{\partial \phi_i}{\partial y_0} - \rho g_x \phi_i + \rho \left(u_0 \frac{\partial u_0}{\partial \Gamma} \frac{\partial x_0}{\partial \Gamma} + v_0 \frac{\partial u_0}{\partial \Gamma} \frac{\partial y_0}{\partial \Gamma} \right) \phi_i \right.$$

$$+ 2\mu \frac{\partial u_0}{\partial \Gamma} \frac{\partial x_0}{\partial \Gamma} \frac{\partial \phi_i}{\partial x_0} + \left(-p_0 + 2\mu \frac{\partial u_0}{\partial x_0} \right) \frac{\partial x_0}{\partial \Gamma} \frac{\partial \phi_i}{\partial \Gamma} + \mu \left(\frac{\partial u_0}{\partial y_0} + \frac{\partial v_0}{\partial x_0} \right) \frac{\partial y_0}{\partial \Gamma} \frac{\partial \phi_i}{\partial \Gamma}$$

$$\left. + \mu \left(\frac{\partial u_0}{\partial \Gamma} \frac{\partial y_0}{\partial \Gamma} + \frac{\partial v_0}{\partial \Gamma} \frac{\partial x_0}{\partial \Gamma} \right) \frac{\partial \phi_i}{\partial y_0} \right\} \phi_j \, d\Gamma + \sigma \int_{\Gamma_{fs}} \left\{ n_{0x} \frac{\partial \phi_i}{\partial \Gamma} \frac{\partial \phi_j}{\partial \Gamma} + \frac{\partial n_{0x}}{\partial \Gamma} \frac{\partial \phi_i}{\partial \Gamma} \phi_j \right.$$

$$- N^2 \frac{\partial y_0}{\partial \Gamma} \left(n_{0y} \frac{\partial x_0}{\partial \Gamma} - n_{0x} \frac{\partial y_0}{\partial \Gamma} \right) \phi_i \phi_j - \frac{\partial x_0}{\partial \Gamma} \left(n_{0y} \frac{\partial y_0}{\partial \Gamma} + n_{0x} \frac{\partial x_0}{\partial \Gamma} \right) \frac{\partial \phi_i}{\partial \Gamma} \frac{\partial \phi_j}{\partial \Gamma}$$

$$\left. - \frac{\partial x_0}{\partial \Gamma} \left(\frac{\partial n_{0y}}{\partial \Gamma} \frac{\partial y_0}{\partial \Gamma} + \frac{\partial n_{0x}}{\partial \Gamma} \frac{\partial x_0}{\partial \Gamma} \right) \frac{\partial \phi_i}{\partial \Gamma} \phi_j \right\} d\Gamma$$

(II) y-Component of Momentum Equation

$$M_{v'_i,v'_j} = -\int_\Omega \rho \phi_i \phi_j \, d\Omega$$

Continued

TABLE I—*Continued*

$$J_{v_i',u_j'} = \int_\Omega \left\{ \rho \frac{\partial v_0}{\partial x_0} \phi_j \phi_i + \mu \frac{\partial \phi_j}{\partial y_0} \frac{\partial \phi_i}{\partial x_0} \right\} d\Omega - \int_{\Gamma_{in}} \frac{\partial \phi_j}{\partial y_0} \phi_i n_{0x}\, \partial\Gamma - \int_{\Gamma_{out}} \frac{\partial \phi_j}{\partial y_0} \phi_i n_{0x}\, d\Gamma$$

$$J_{v_i',v_j'} = \int_\Omega \left\{ \rho \left(u_0 \frac{\partial \phi_j}{\partial x_0} + v_0 \frac{\partial \phi_j}{\partial y_0} + \frac{\partial v_0}{\partial y_0} \phi_j \right) \phi_i + \mu \frac{\partial \phi_j}{\partial x_0} \frac{\partial \phi_i}{\partial x_0} + 2\mu \frac{\partial \phi_j}{\partial y_0} \frac{\partial \phi_i}{\partial y_0} + N^2 \mu \phi_i \phi_j \right\} d\Omega$$

$$- \int_{\Gamma_{in}} \left\{ \frac{\partial \phi_j}{\partial x_0} \phi_i n_{0x} + 2 \frac{\partial \phi_j}{\partial y_0} \phi_i n_{0y} \right\} d\Gamma - \int_{\Gamma_{out}} \frac{\partial \phi_j}{\partial y_0} \phi_i n_{0y}\, d\Gamma$$

$$J_{v_i',w_j'} = - \int_\Omega N \mu \frac{\partial \phi_j}{\partial y_0} \phi_i\, d\Omega$$

$$J_{v_i',p_j'} = - \int_\Omega \frac{\partial \phi_i}{\partial y_0} \chi_j\, d\Omega + \int_{\Gamma_{out}} \chi_j \phi_i n_{0y}\, d\Gamma$$

$$J_{v_i',h_j'} = \int_{\Gamma_{fs}} \left\{ -2\mu \frac{\partial v_0}{\partial y_0} \frac{\partial \phi_i}{\partial y_0} - \mu \left(\frac{\partial u_0}{\partial y_0} + \frac{\partial v_0}{\partial x_0} \right) \frac{\partial \phi_i}{\partial x_0} - \rho g_y \phi_i + \rho \left(u_0 \frac{\partial v_0}{\partial \Gamma} \frac{\partial x_0}{\partial \Gamma} + v_0 \frac{\partial v_0}{\partial \Gamma} \frac{\partial y_0}{\partial \Gamma} \right) \phi_i \right.$$

$$+ 2\mu \frac{\partial v_0}{\partial \Gamma} \frac{\partial y_0}{\partial \Gamma} \frac{\partial \phi_i}{\partial y_0} + \left(-p_0 + 2\mu \frac{\partial v_0}{\partial y_0} \right) \frac{\partial y_0}{\partial \Gamma} \frac{\partial \phi_i}{\partial \Gamma} + \mu \left(\frac{\partial u_0}{\partial y_0} + \frac{\partial v_0}{\partial x_0} \right) \frac{\partial x_0}{\partial \Gamma} \frac{\partial \phi_i}{\partial \Gamma}$$

$$\left. + \mu \left(\frac{\partial u_0}{\partial \Gamma} \frac{\partial y_0}{\partial \Gamma} + \frac{\partial v_0}{\partial \Gamma} \frac{\partial x_0}{\partial \Gamma} \right) \frac{\partial \phi_i}{\partial x_0} \right\} \phi_j\, d\Gamma + \sigma \int_{\Gamma_{fs}} \left\{ n_{0y} \frac{\partial \phi_i}{\partial \Gamma} \frac{\partial \phi_j}{\partial \Gamma} + \frac{\partial n_{0y}}{\partial \Gamma} \frac{\partial \phi_i}{\partial \Gamma} \phi_j \right.$$

$$+ N^2 \frac{\partial x_0}{\partial \Gamma} \left(n_{0y} \frac{\partial x_0}{\partial \Gamma} - n_{0x} \frac{\partial y_0}{\partial \Gamma} \right) \phi_i \phi_j - \frac{\partial y_0}{\partial \Gamma} \left(n_{0y} \frac{\partial y_0}{\partial \Gamma} + n_{0x} \frac{\partial x_0}{\partial \Gamma} \right) \frac{\partial \phi_i}{\partial \Gamma} \frac{\partial \phi_j}{\partial \Gamma}$$

$$\left. - \frac{\partial y_0}{\partial \Gamma} \left(\frac{\partial n_{0y}}{\partial \Gamma} \frac{\partial y_0}{\partial \Gamma} + \frac{\partial n_{0x}}{\partial \Gamma} \frac{\partial x_0}{\partial \Gamma} \right) \frac{\partial \phi_i}{\partial \Gamma} \phi_j \right\} d\Gamma$$

I) z-Component of Momentum Equation

$$M_{w_i'},\, w_j' = - \int_\Omega \rho \phi_i \phi_j\, d\Omega$$

$$J_{w_i',u_j'} = - \int_\Omega N \mu \frac{\partial \phi_i}{\partial x_0} \phi_j\, d\Omega - \int_{\Gamma_{in}} N \phi_j \phi_i n_{0x}\, d\Gamma - \int_{\Gamma_{out}} N \phi_j \phi_i n_{0x}\, d\Gamma$$

$$J_{w_i',v_j'} = - \int_\Omega N \mu \frac{\partial \phi_i}{\partial y_0} \phi_j\, d\Omega - \int_{\Gamma_{in}} N \phi_j \phi_i n_{0y}\, d\Gamma - \int_{\Gamma_{out}} N \phi_j \phi_i n_{0y}\, d\Gamma$$

$$J_{w_i',w_j'} = - \int_\Omega \left\{ \rho \left(u_0 \frac{\partial \phi_j}{\partial x_0} + v_0 \frac{\partial \phi_j}{\partial y_0} \right) \phi_i + \mu \frac{\partial \phi_j}{\partial x_0} \frac{\partial \phi_i}{\partial x_0} + \mu \frac{\partial \phi_j}{\partial y_0} \frac{\partial \phi_i}{\partial y_0} + 2N^2 \mu \phi_i \phi_j \right\} d\Omega$$

$$J_{w_i',p_j'} = - \int_\Omega N \phi_i \chi_j\, d\Omega$$

$$J_{w_i',h_j'} = - \int_{\Gamma_{fs}} N p_0 \phi_i \phi_j\, d\Gamma + \sigma N \int_{\Gamma_{fs}} \left\{ \phi_i \frac{\partial \phi_j}{\partial \Gamma} \left(n_{0y} \frac{\partial y_0}{\partial \Gamma} + n_{0x} \frac{\partial x_0}{\partial \Gamma} \right) \right.$$

$$\left. + \phi_i \phi_j \left(\frac{\partial n_{0y}}{\partial \Gamma} \frac{\partial y_0}{\partial \Gamma} + \frac{\partial n_{0x}}{\partial \Gamma} \frac{\partial x_0}{\partial \Gamma} \right) + \phi_j \frac{\partial \phi_i}{\partial \Gamma} \left(n_{0y} \frac{\partial y_0}{\partial \Gamma} + n_{0x} \frac{\partial x_0}{\partial \Gamma} \right) \right\} d\Gamma$$

Continued

TABLE I—*Continued*

(IV) Continuity Equation

$$J_{p'_i,u'_j} = -\int_\Omega \frac{\partial \phi_j}{\partial x_0}\chi_i \, d\Omega$$

$$J_{p'_i,v'_j} = -\int_\Omega \frac{\partial \phi_j}{\partial y_0}\chi_i \, d\Omega$$

$$J_{p'_i,w'_j} = -\int_\Omega N\phi_j \chi_i \, d\Omega$$

$$J_{p'_i,h'_j} = \int_{\Gamma_{fs}} \left(\frac{\partial x_0}{\partial \Gamma}\frac{\partial u_0}{\partial \Gamma} + \frac{\partial y_0}{\partial \Gamma}\frac{\partial v_0}{\partial \Gamma}\right)\chi_i \phi_j \, d\Gamma$$

(V) Free Boundary Perturbation

Kinematic boundary condition at free surface

$$M_{h'_i,h'_j} = \int_{\Gamma_{fs}} \phi_i \phi_j \, d\Gamma$$

$$J_{h'_i,u'_j} = \int_{\Gamma_{fs}} n_{0x}\phi_i \phi_j \, d\Gamma$$

$$J_{h'_i,v'_j} = \int_{\Gamma_{fs}} n_{0y}\phi_i \phi_j \, d\Gamma$$

$$J_{h'_i,h'_j} = -\int_{\Gamma_{fs}} \left[u_0 \frac{\partial x_0}{\partial \Gamma} + v_0 \frac{\partial y_0}{\partial \Gamma}\right]\phi_i \frac{\partial \phi_j}{\partial \Gamma} \, d\Gamma$$

Force balance at deformable wall surface

$$J_{h'_i,u'_j} = \int_{\Gamma_d} \frac{1}{K}\left\{2\mu \frac{\partial \phi_j}{\partial x_0} n_{0x} N_{0x} + \mu \frac{\partial \phi_j}{\partial y_0} n_{0y} N_{0x} + \mu \frac{\partial \phi_j}{\partial y_0} n_{0x} N_{0y}\right\}\overline{\phi_i} \, d\Gamma$$

$$J_{h'_i,v'_j} = \int_{\Gamma_d} \frac{1}{K}\left\{2\mu \frac{\partial \phi_j}{\partial y_0} n_{0y} N_{0y} + \mu \frac{\partial \phi_j}{\partial x_0} n_{0y} N_{0x} + \mu \frac{\partial \phi_j}{\partial x_0} n_{0x} N_{0y}\right\}\overline{\phi_i} \, d\Gamma$$

$$J_{h'_i,p'_j} = -\int_{\Gamma_d} \frac{1}{K}(n_{0x} N_{0x} + n_{0y} N_{0y})\chi_j \overline{\phi_i} \, d\Gamma$$

$$\begin{aligned} J_{h'_i,h'_j} = -\int_{\Gamma_d} \Bigg\{ & \frac{1}{K}\Bigg\{ N_{0x}\frac{\partial \phi_j}{\partial \Gamma}\frac{\partial n_{0y}}{\partial \Gamma}\left[-p_0 + 2\mu\frac{\partial u_0}{\partial x_0} + \mu\left(\frac{\partial u_0}{\partial y_0} + \frac{\partial v_0}{\partial x_0}\right)\right] \\ & + N_{0y}\frac{\partial \phi_j}{\partial \Gamma}\frac{\partial n_{0x}}{\partial \Gamma}\left[-p_0 + 2\mu\frac{\partial v_0}{\partial y_0} + \mu\left(\frac{\partial u_0}{\partial y_0} + \frac{\partial v_0}{\partial x_0}\right)\right] + \frac{1}{|\mathbf{J_0}|}\Bigg[-2\mu\frac{\partial u_0}{\partial x_0}n_{0x}N_{0x} \\ & - 2\mu\frac{\partial v_0}{\partial y_0}n_{0y}N_{0y} - \mu\left(\frac{\partial u_0}{\partial y_0} + \frac{\partial v_0}{\partial x_0}\right)(n_{0y}N_{0x} + n_{0x}N_{0y})\Bigg]\Bigg[\frac{\partial y_0}{\partial \Gamma^t}\left(\frac{\partial \phi_j}{\partial \Gamma}n_{0x} + \phi_j\frac{\partial n_{0x}}{\partial \Gamma}\right) \\ & - \frac{\partial x_0}{\partial \Gamma^t}\left(\frac{\partial \phi_j}{\partial \Gamma}n_{0y} + \phi_j\frac{\partial n_{0y}}{\partial \Gamma}\right)\Bigg] + \frac{1}{|\mathbf{J_0}|}\Bigg[-2\mu n_{0x}N_{0x}\frac{\partial u_0}{\partial \Gamma^t}\left(\frac{\partial \phi_j}{\partial \Gamma}n_{0y} + \phi_j\frac{\partial n_{0y}}{\partial \Gamma}\right) \\ & + \mu(n_{0y}N_{0x} + n_{0x}N_{0y})\left(\frac{\partial u_0}{\partial \Gamma^t}\left(\frac{\partial \phi_j}{\partial \Gamma}n_{0x} + \phi_j\frac{\partial n_{0x}}{\partial \Gamma}\right) - \frac{\partial v_0}{\partial \Gamma^t}\left(\frac{\partial \phi_j}{\partial \Gamma}n_{0y} + \phi_j\frac{\partial n_{0y}}{\partial \Gamma}\right)\right) \\ & + 2\mu n_{0y}N_{0y}\frac{\partial v_0}{\partial \Gamma^t}\left(\frac{\partial \phi_j}{\partial \Gamma}n_{0x} + \phi_j\frac{\partial n_{0x}}{\partial \Gamma}\right)\Bigg]\Bigg\} + \phi_j(n_{0x}N_{0x} + n_{0y}N_{0y})\Bigg\}\overline{\phi_i} \, d\Gamma \end{aligned}$$

4.3. Method of Solving the Generalized Eigenproblem

The stability of the flow is dictated by the eigenvalues with largest real parts, the *leading eigenvalues*. Therefore, all that are needed from (12) are those eigenvalues that are, or are candidates to become, the leading ones. The eigenfunctions are often of interest, too.

When the mass matrix **M** is singular and the Jacobian **J** is nonsingular, the number of eigenvalues is smaller than the dimension of the problem (see Golub and Van Loan [17]). The number of missing eigenvalues is equal to the number of equations that lead to an identically zero row in the mass matrix. These equations are those that do not present time derivatives, i.e., the algebraic equations related with the continuity equation, essential boundary conditions, and force balance at the deformable wall.

As explained by Christodoulou and Scriven [8], the missing eigenvalues are generally referred to as "infinite eigenvalues" because if **M** is perturbed such that it becomes nonsingular, very large eigenvalues appear and they grow as the perturbation is reduced. So, when searching for the leading eigenvalues that dictate the stability of the problem, these effectively infinite eigenvalues have to be removed from the equation system, for otherwise they are the ones with largest real part. A way of accomplishing this is by using a transformation that maps them to zero. An example of such transformation is the shift-and-invert transformation. The generalized eigenproblem is rewritten in terms of a shift γ, which for the present purpose is real. The transformed eigenproblem becomes

$$\mathbf{A}\mathbf{c}' = \mu\mathbf{c}'; \qquad \mathbf{A} = (\mathbf{J} - \gamma\mathbf{M})^{-1} \text{ and } \mu = \frac{1}{\beta - \gamma}. \tag{13}$$

The infinite eigenvalues of the generalized problem are mapped into zero eigenvalues of the simple eigenvalue problem, i.e., $\mu = 0$, when $\beta = \infty$. In this way, too, the generalized eigenproblem (12) is altered to a simple eigenproblem, Eq. (13). The leading eigenvalues of (13) are those eigenvalues of the original problem that are closet to the shift value γ, i.e., μ is maximum when $\beta - \gamma$ is minimum.

Equation (13) was solved by an iterative Arnoldi method with implicit deflation developed by Saad [29] for asymmetric eigenproblems.

4.4. Test Problems

Before this method was used to find the stability of flows in deformable roll coating gaps, it was tried on two free surface problems for which solutions are available in the literature. The first was the stability of a static liquid layer, a quite simple example. The second problem was the stability of film-splitting flows between rigid rolls.

4.4.1. *Static Liquid Layer*

This is a simple test because the base state consists of zero velocity, hydrostatic pressure distribution, and flat free surface. Liquid fills a rectangular pool of width L and height D (see Fig. 7); the aspect ratio of $L/D = 5$ was chosen. The contact lines were prescribed to be pinned.

The stability with respect to three-dimensional disturbances of wavenumber $ND \geq 0.0628$ was computed. Because the disturbance in the transverse direction is taken to be periodic, there was no need of including a volume constrain to the system of equations. Ruschak [25] confirmed that if the mesh is well refined, the results for this aspect ratio match to desired accuracy the leading eigenvalue, which is real, of the analytical solution in the limiting case

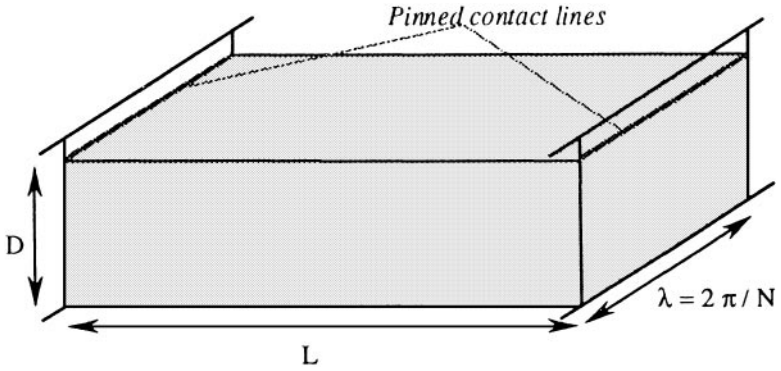

FIG. 7. Rectangular liquid pool of width L and depth D. The contact lines are pinned.

of a infinitely wide liquid layer (Anshus, [1]):

$$\beta = -\left(1 + \frac{N^2}{Bo}\right)\frac{\cosh N \sinh N - N}{2N(N^2 + \cosh^2 N)}.$$

$Bo \equiv \rho g D^2/\sigma$ is the Bond number, which gives the ratio between gravitational and capillary forces. Provided gravity is directed downwards, all eigenvalues are negative, i.e., the base state is stable.

The domain was divided into 50 elements by a 5×10 mesh. Figure 8 compares the real part of the eigenvalue computed as a function of wavenumber N at $Bo = 1$ with the analytical solution of Anshus [1] and results of Christodoulou [9]. The agreement is good over the entire range of wavenumbers. With the 50-element mesh, the size of the matrix eigenproblem is 864×864. Had the location of internal nodes been perturbed, following

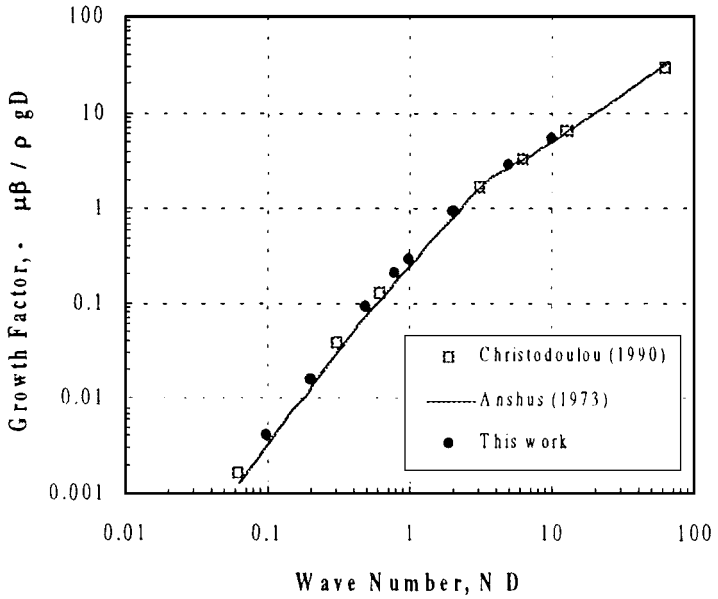

FIG. 8. Growth factor β of three-dimensional sinusoidal perturbation in the transverse direction as a function of the wavenumber of the disturbance. $Bo = 1$.

the approach used by Christodoulou and Scriven [8], the size of the matrix eigenproblem for the same discretization would have been 1305×1305.

4.4.2. *Film-Splitting Flows between Rigid Rolls*

In this second test flow, liquid is dragged through the gap between two counter-rotating rigid rolls and then splits into two films, one attached to each roll. Coyle *et al.* [12] analyzed the stability of this flow by means of the Galerkin/finite element method. Because they followed Ruschak [25] in neglecting the local accelaration within the liquid, their formulation is strictly correct only at zero Reynolds number or at the condition of marginal instability of non-periodic normal modes. Their results at vanishing Reynolds number are the basis of comparison here.

The boundary conditions are the same as the ones used for the deformable roll gap presented before, with the exclusion of the resilient roll.

The eigenvalues with largest real part were computed at different wavenumbers of the periodic transverse disturbance. At all the conditions explored, the leading eigenvalue had no significant imaginary part, as illustrated in Fig. 9. The figure shows the first ten leading eigenvalues (largest real part) at a gap to diameter ratio $H_0/R = 2 \times 10^{-2}$, capillary number $Ca = 2$, and wavenumber $NH_0 = 0.1$. Because the real part of the leading eigenvalue is negative, the flow is stable with respect to this particular perturbation.

Figure 10 plots the computed growth factor β as a function of wavenumber N at the gap $H_0/R = 2 \times 10^{-2}$, vanishing Reynolds number, and different capillary numbers. At $Ca = 0.5$, β is negative at all wavenumbers $N = 2\pi/\lambda$, i.e., the flow is stable with respect to all three-dimensional infinitesimal perturbations. At $Ca = 10$, β is positive over a range of N, i.e., the corresponding perturbations grow exponentially with time. Though the steady-state seen in experiments is a secondary flow governed by nonlinear effects (Gurfinkel and Patera [18]), its wavenumber appears to be close to that of the normal mode with largest β, i.e., the one that grows fastest. At $Ca = 10$, that wavenumber is approximately $NH_0 = 0.35$.

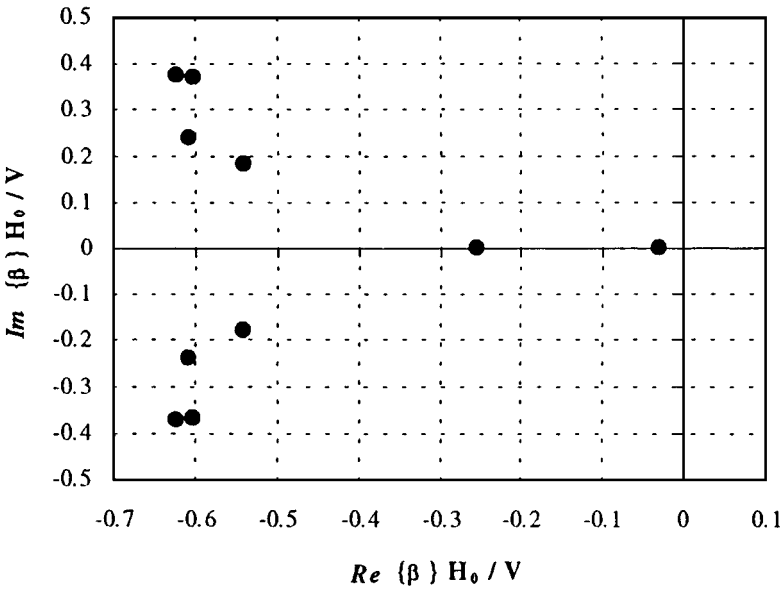

FIG. 9. Eigenvalues with largest real part for film-splitting flow between rigid rolls at a gap to diameter ratio $H_0/R = 2 \times 10^{-2}$, capillary number $Ca = 2$, and wavenumber $NH_0 = 0.1$.

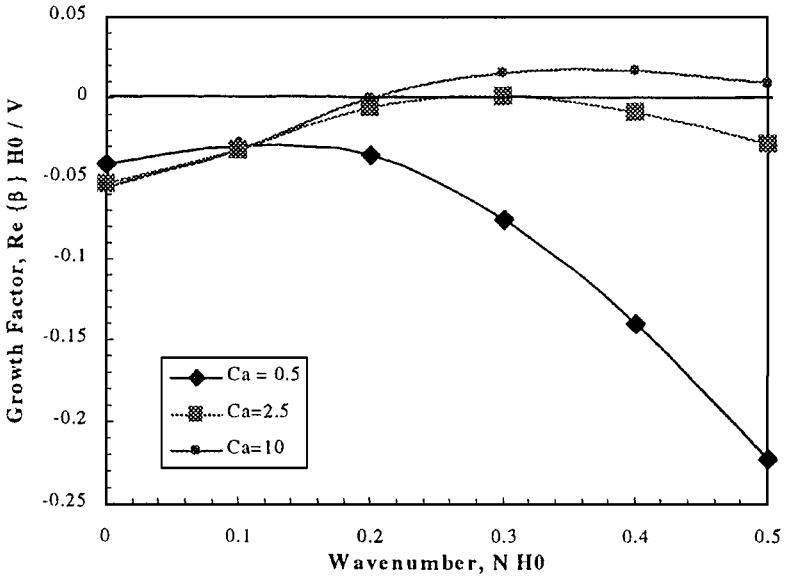

FIG. 10. Growth factor versus wavenumbers at various capillary numbers for the film-splitting flow between rigid rolls. $Re \equiv \rho V H_0/\mu = 0$ and gap to roll diameter ratio $H_0/R = 2 \times 10^{-2}$. The critical capillary number for the onset of ribbing instability is about $Ca^* = 2.5$. The leading eigenvalue was real for all the cases analyzed.

At about $Ca = 2.5$, that wavenumber is approximately $N H_0 = 0.3$, but the curve is tangent to the $\Re\{\beta\} = 0$ line: the growth rate is zero. This defines the *critical capillary number*. Above it, the two-dimensional flow is unstable with respect to the class of perturbations covered by the analysis; below it, the flow is stable with respect to all such perturbations.

Figure 11 reports the results of computing a critical capillary number versus the ratio of gap $2H_0$ to diameter $2R$, i.e., the predicted critical condition at each roll separation.

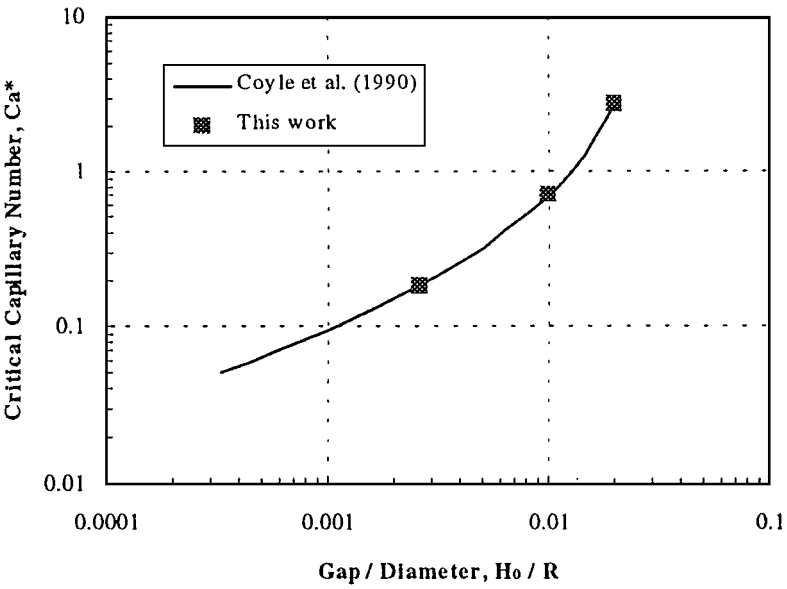

FIG. 11. Critical capillary number for the onset of ribbing as a function of gap to roll diameter ratio at $Re = 0$. The continuous line shows the theoretical predictions reported by Coyle *et al.* [12]; the squares are predictions with the computationally more efficient method developed in this work.

Above the curve of a critical capillary number, the flow is unstable with respect to perturbations that lead to ribbing. The predictions of a critical capillary number computed in this work agree with interpolations of Coyle *et al.* [12]. Though the comparison is at the vanishing Reynolds number, the formulation in the present work is not restricted to this limit. No independent results at non-zero Reynolds number were accessible, however.

The size of the eigenproblem for the 352-element mesh used was 5696×5696. Had the locations of internal nodes been perturbed, following the approach of Christodoulou and Scriven [8], the size of the eigenproblem, with the same discretization, would have been 8681×8681. At the same level of accuracy, the matrix dimension of the eigenproblem is only 65% of that when the earlier approach was used. This translates into a substantial saving of memory and computational time required to solve the matrix eigenproblem, Eq. (12).

5. CRITICAL CAPILLARY NUMBERS IN A DEFORMABLE ROLL COATING GAP

The issue here is the effect of a deformable roll or roll cover on the stability of film-splitting flow.

First, the stability of the flow between rigid rolls is compared with the stability of the flow in a deformable gap at the same operating conditions. Figure 12 illustrates how the real part of the leading eigenvalue for both rigid and a deformable gaps varies with wavenumber at $H_0/R = 2.6 \times 10^{-3}$ and $Ca = 0.2$. As mentioned before, the leading eigenvalues had no significant imaginary part.

The elasticity number of the deformable roll case was $Ne^* \equiv \mu \bar{V}/K R^2 = 10^{-6}$, that represents a soft roll cover. For this set of conditions, the flow between rigid rolls is unstable—there is a small range of wavenumbers N such that the growth factor β is positive—and the flow in the deformable gap is stable. This result indicates that the roll deformation delays the onset of ribbing, even when the rolls are not in interference, i.e., a positive gap.

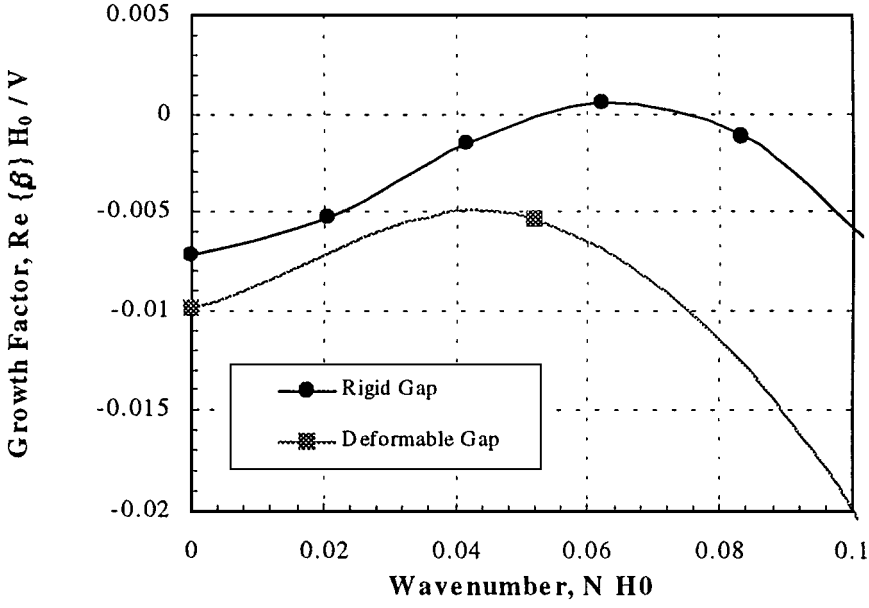

FIG. 12. Leading eigenvalue as a function of wavenumber $N \equiv 2\pi/\lambda$ (λ is the wavelength of the disturbance) at gap-to-diameter ratio $H_0/R = 2.6 \times 10^{-3}$ and capillary number $Ca = 0.2$: (a) Rigid gap, and (b) deformable gap ($Ne^* = 10^{-6}$). The leading eigenvalue was real in all the cases analyzed.

The critical capillary number Ca^* was determined by locating the growth factor curve that is tangent to the horizontal axis at each ratio of gap to roll diameter, $2H_0/2R$. Figure 13 illustrates this process by showing the growth factor versus wavenumber at modified elasticity number $Ne^* = 10^{-6}$ and gaps of $H_0/R = 2.6 \times 10^{-3}$ and $H_0/R = 4.3 \times 10^{-4}$ at different capillary numbers. The critical capillary number at the first gap-to-roll radius ratio was $Ca^* = 0.28$, and at the second, $Ca^* = 0.25$. The critical value for the onset of ribbing decreases with the gap between the rolls, as expected.

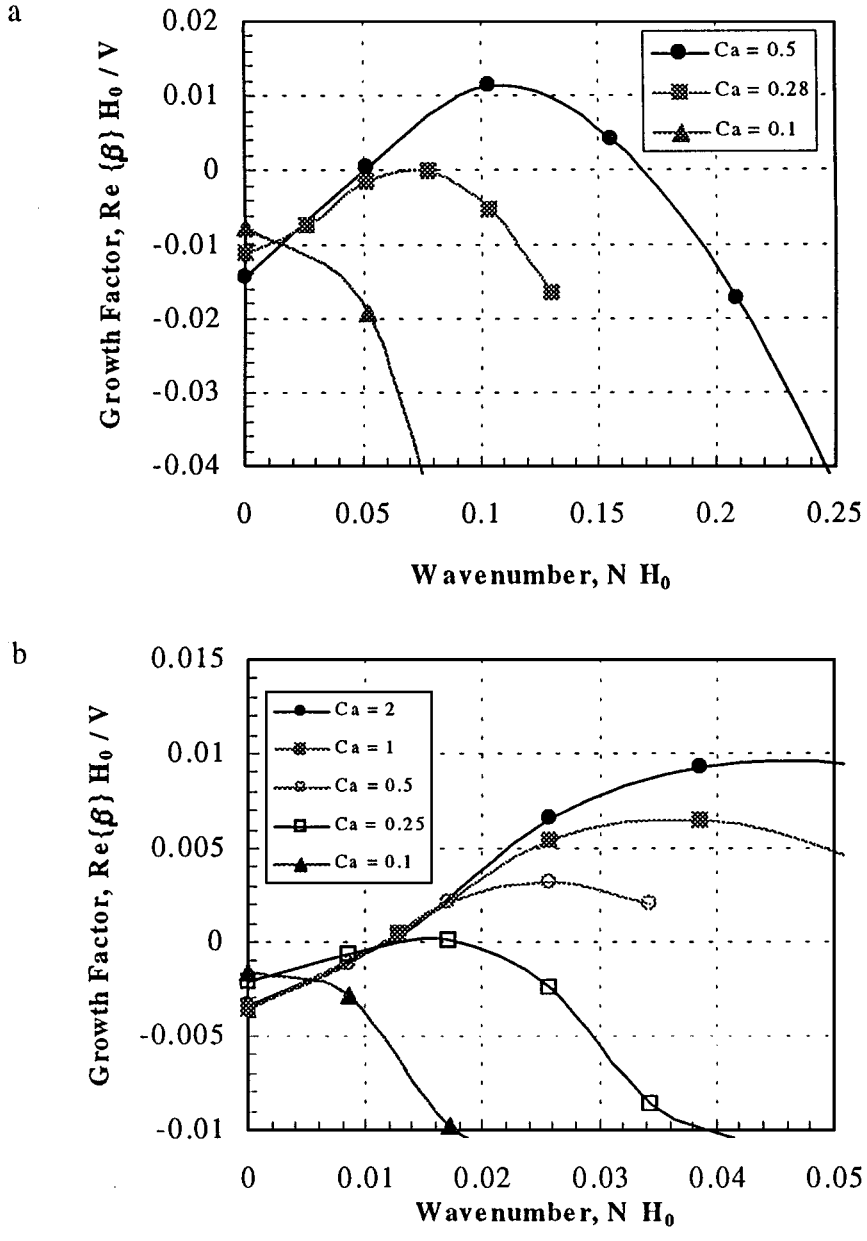

FIG. 13. Leading eigenvalue as a function of wavenumber $N \equiv 2\pi/\lambda$ (λ is the wavelength of the disturbance) at modified elasticity number $Ne^* = 10^{-6}$. (a) $H_0/R = 2.6 \times 10^{-3}$ and (b) $H_0/R = 4.3 \times 10^{-4}$.

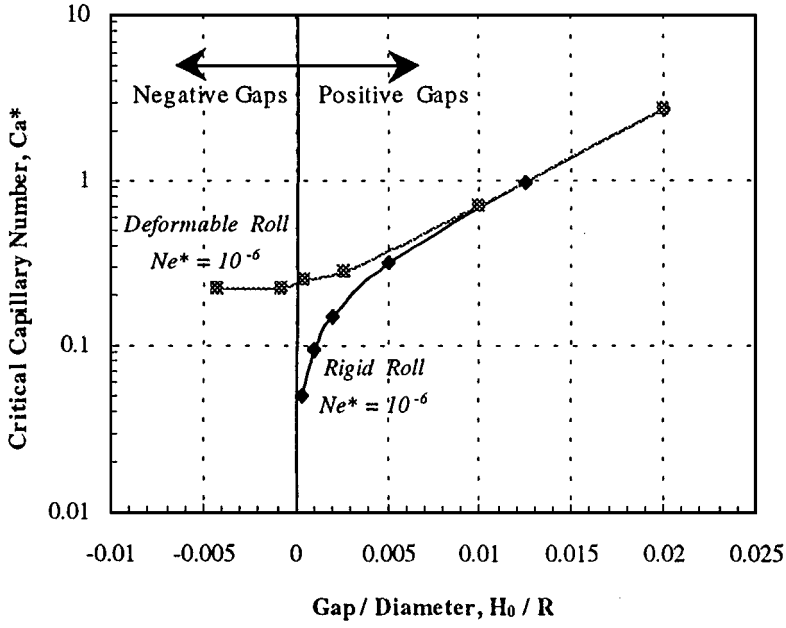

FIG. 14. Critical capillary number versus gap-to-roll diameter ratio for rigid and deformable gaps. Negative gaps correspond to the situation when the distance between the roll axes is smaller than the sum of the roll radii.

The critical capillary number is plotted against gap-to-roll diameter in Fig. 14 at $Ne^* = 10^{-6}$. The results include negative gaps, i.e., when the distance between the roll axes is smaller than the sum of the undeformed roll radii and so the rolls at rest would be in interference. The critical capillary numbers for a film-splitting flow between rigid rolls are shown for comparison. When the gap setting is large ($H_0/R > 10^{-1}$), the liquid pressure is not enough to deform the roll cover appreciably and the deformable roll behaves as if it were rigid. As the gap between the rolls is narrowed, the pressure in the liquid between them rises, and the rubber cover deforms in response. At a given distance between the roll axes, the critical capillary numbers in a deformable gap, e.g., $Ne^* = 10^{-6}$, are always larger than those in a rigid gap. Thus, at a fixed distance between the roll axes, a deformable gap can produce a uniform film at higher speeds of operation. As described elsewhere (Carvalho and Scriven [5]), the deformation of the resilient roll elongates the gap and pushes the film-split meniscus further downstream, thereby lessening the pressure gradient in the liquid at the curved free surface at the splitting film. The lower the pressure gradient there, the more stable the flow. When the roll cover is very soft (large elasticity number, viz. $Ne^* = 10^{-6}$), the critical capillary number is high and its sensitivity to gap is small. At negative gaps, the critical capillary number scarcely changes at all as the rolls are moved further together: it falls by less than 2% as the interference goes from $H_0/R = -7.5 \times 10^{-4}$ to -4.5×10^{-3}.

The wavelength of the fastest growing disturbance at capillary numbers beyond the critical value is of some interest. The ribbing instability that develops in the film split and is carried downstream by the coated layers appears to have about this wavelength. The rate at which the nonuniform coated layer subsequently levels is a function of the curvature of the film, and therefore a function of the wavelength of the ribbing. If the disturbance wavelength is not too long, the leveling rate is inversely proportional to the fourth power of that wavelength (Anshus [1]). Figures 10, 12, and 13 also show the growth factor versus wavenumber for

capillary numbers above the critical values for both rigid and deformable gaps. In all cases, the wavenumber of the fastest growing perturbation grows as the capillary number is raised. Beyond the onset of ribbing, if the roll speed is raised further, the wavelength $\lambda \equiv 2\pi/N$ of the ribbing disturbance shortens, which fastens leveling.

The effect on film uniformity can be profound and paradoxical: Ultimate smoothness may be enhanced by raising the roll speed. Figure 15 shows the wavelength $\lambda \equiv 2\pi/N$ of the fastest growing disturbance in units of half-gap H_0 versus capillary number at different gap to roll diameter ratio, for both rigid and deformable gaps. Interestingly, when the rolls

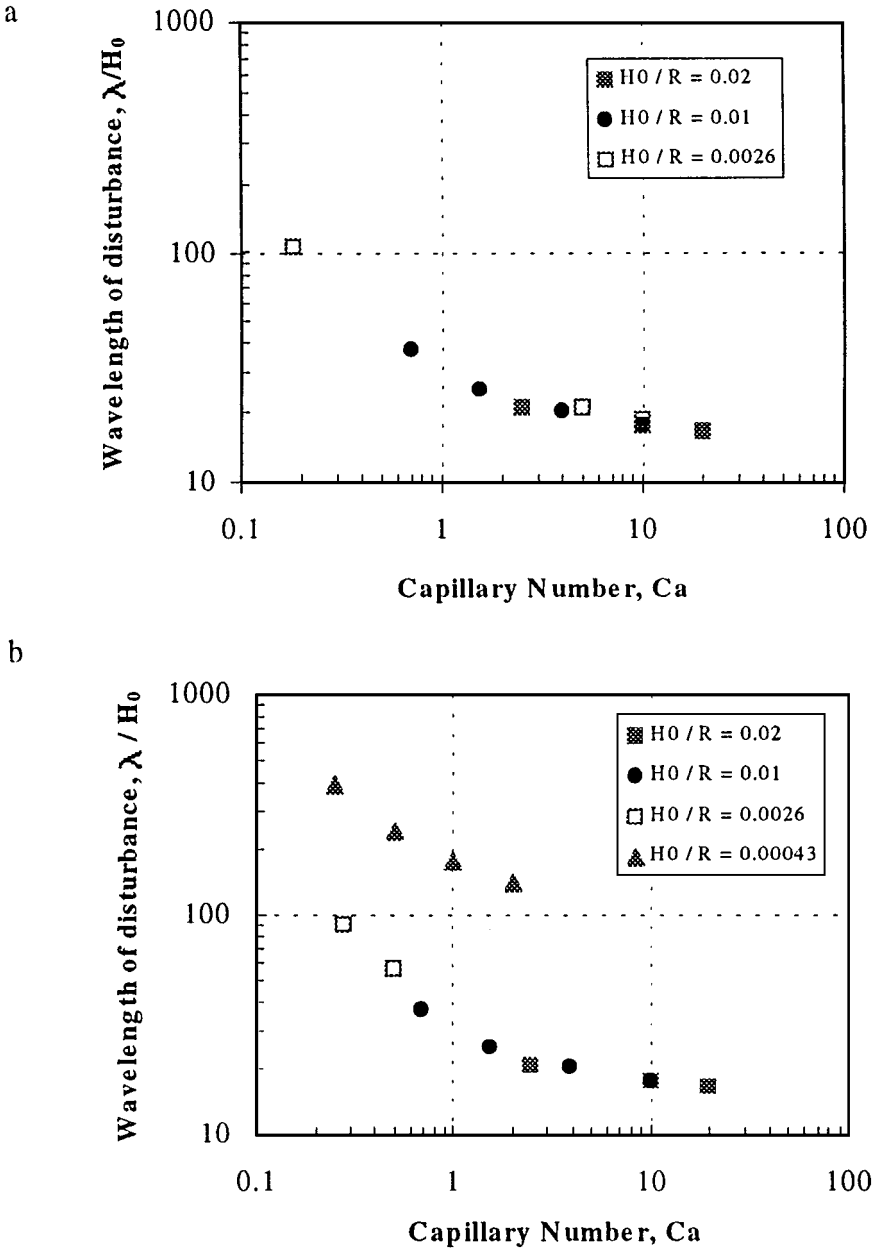

FIG. 15. Wavelength in units of half gap λ/H_0 of three-dimensional disturbance from (a) rigid gaps and (b) deformable gaps.

are rigid, the predictions for different gaps (H_0/R) come close to all lieing on a single curve. At low capillary number ($Ca < 1$), the sensitivity of wavelength to capillary number is strong. If the capillary number is raised from $Ca = 0.1$ to $Ca = 0.2$, the wavelength to gap ratio falls from $\lambda/H_0 \approx 100$ to $\lambda/H_0 \approx 60$. However, at large capillary numbers ($Ca > 10$), the sensitivity falls and the single curve that represents all gaps asymptotically approaches a wavelength to gap ratio of $\lambda/H_0 \approx 15$. The results from the analysis of the soft-roll case are the same as those from the rigid-roll case when the gap setting is large. The liquid pressure is not enough to deform the roll cover appreciably and the deformable roll behaves as if it were rigid. When the roll cover deformation is appreciable, i.e. when the gap is small or negative, there is a major difference: at the same capillary number the wavelength generated by deformable gaps is greater than that generated by rigid gaps. Consequently the rate of leveling of the coated film downstream of the film-split may be substantially smaller when a deformable gap is used. These theoretical inferences agree qualitatively with measurements of ribbing wavelengths that are reported by Pulkrabek and Munter [24] and Carvalho *et al.* [4].

In the foregoing discussion, the comparisons between the behavior of rigid and deformable gaps (Fig. 14) are at the same distance between the axes of the rolls, i.e., H_0/R. However, at a given gap H_0/R, the flow rate through a deformable gap is larger than between rigid ones, because the resilient roll cover is compressed by the pressure that develops in the flowing liquid. In practice, a certain thickness of coated layer or film is desired, and the gap or roll loading is adjusted to meet the specification. Hence it is appropriate to compare gap performances on the basis of fixed layer thicknesses, or flow rate, but different axis to axis distances. To do so requires combining flow rate predictions at different gaps and modified elasticity numbers (see Carvalho and Scriven [5]) with predictions of critical capillary number (Fig. 14). The result of doing this is shown in Fig. 16. The curve for the

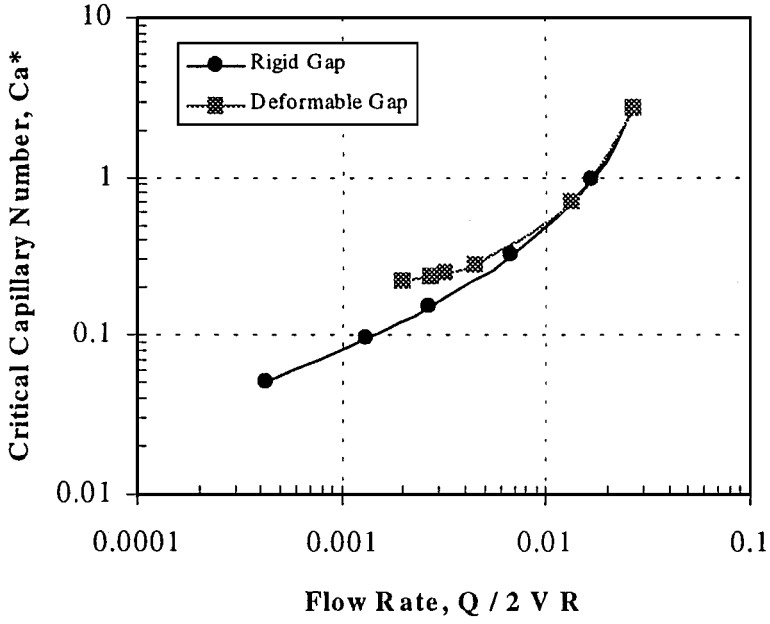

FIG. 16. Comparison of critical capillary number from rigid and deformable gaps as a function of the coated layer thickness in units of roll radius, $t/R = Q/2VR$.

deformable gap ($Ne^* = 10^{-6}$, i.e., soft roll cover) does not extend to flow rates less than approximately $Q/2\bar{V}R = 2 \times 10^{-3}$. With soft roll covers and negative gaps, the flow rate is nearly insensitive to the position or loading of the rolls. After a certain point, raising the loading or decreasing the distance between the roll axes does not decrease the flow rate appreciably. Therefore, a very small flow rate cannot be obtained with a very soft roll cover (see Carvalho and Scriven [5]). At a given flow rate, that can be translated to a coated film thickness, the critical capillary numbers in deformable gaps are larger than those in rigid gaps. For example, if a flow rate of $Q/2\bar{V}R = 2 \times 10^{-3}$ is specified, a smooth coated film can be obtained with a rigid roll at capillary numbers up to approximately $Ca^* \approx 0.105$. If a deformable roll with a modified elasticity number $Ne^* = 10^{-6}$ is used, the maximum capillary number is approximately $Ca^* \approx 0.205$. In summary, the gap between a soft roll and a hard one of the same diameter and speed can be expected to produce perfectly smooth coating at a speed almost twice as fast as the gap between a pair of rigid rolls.

6. FINAL REMARKS

The operability limits of coating processes are usually restricted by hydrodynamic instabilities that produce defects on the coated film. A way of predicting theoretically these limits is to study the stability of two-dimensional steady flows with respect to infinitesimal disturbances. The mathematical formulation of the problem leads to large, sparse, and nonsymmetric generalized eigenvalue problems.

A more efficient formulation than the one that has been in use recently was presented. Its essence is to restrict domain perturbations to free boundaries, where they are physically relevant. This approach reduces the size of the eigenproblem. It is also completely independent of the equations used to generate the mesh for solving the two-dimensional steady-state free-surface base flow.

The method was used to study the stability of film-splitting flows in rigid and deformable gaps. The predicted critical capillary numbers for the onset of ribbing from rigid gaps agree with previous results reported by Coyle *et al.* [12]. The results show that the deformation of the roll cover delays the onset of ribbing, i.e., deformable gaps can be operated at higher speeds without producing nonuniform profiles in the cross-web direction.

ACKNOWLEDGMENTS

M. S. Carvalho was supported by a fellowship from CAPES (Brazilian Federal Government). Further support came from cooperating corporations through the Center for Interfacial Engineering and was supplemented by the National Science Foundation and the Minnesota Supercomputer Institute.

REFERENCES

1. B. E. Anshus, The levelling process in a polymer powder painting—A three-dimensional approach, *Am. Chem. Soc. Div. Org. Coating Plastic Chem.* **33**(2), 493 (1973).
2. H. Benkreira, M. F. Edwards, and W. L. Wilkinson, Ribbing instability in the roll coating of Newtonian fluids, *Plastics Rubber Proc. Appl.* **2**, 137 (1982).
3. Bixler, *Stability of a Coating Flow*, Ph.D. thesis, University of Minnesota, University Microfilms International, Ann Arbor, MI, 1982.
4. M. S. Carvalho, T. J. Anderson, and L. E. Scriven, Ribbing instability in forward deformable roll coating, in *Proceedings of 1994 TAPPI Coating Conference, San Diego, 1994*, p. 99.

5. M. S. Carvalho and L. E. Scriven, Deformable roll coating: Modelling of steady flow in gaps and nips, in *First European Coating Symposium on the Mechanics of Thin Film Coating, Leeds, UK, 1995*, p. 221.
6. M. S. Carvalho and L. E. Scriven, Deformable roll coating flows: Steady state and linear perturbation analysis, *J. Fluid Mech.* **339**, 143 (1997).
7. M. S. Carvalho and L. E. Scriven, Flows in forward deformable roll coating gaps: Comparison between spring and plane-strain models of roll cover, *J. Comput. Phys.* **138**(2), 449 (1997).
8. C. N. Christodoulou and L. E. Scriven, Finding leading modes of a viscous free surface flow: An asymmetric generalized eigenproblem, *J. Sci. Comput.* **3**(4), 355 (1988).
9. C. N. Christodoulou, *Computational Physics of Slide Coating Flow*, Ph.D. thesis, University of Minnesota, Minneapolis, 1990.
10. D. J. Coyle, L. E. Scriven, and C. W. Macosko, Film spliting flows in forward roll coating, *J. Fluid Mech.* **171**, 183 (1986).
11. D. J. Coyle, Forward roll coating with deformable rolls: A simple one-dimensional elastohydrodynamic model, *Chem. Eng. Sci.* **43**, 2673 (1988).
12. D. J. Coyle, C. W. Macosko, and L. E. Scriven, Stability of symmetric film-splitting between counter-rotating cylinders, *J. Fluid Mech.* **216**, 437 (1990).
13. J. C. Coyne and H. G. Elrod, Conditions for the rupture of a lubricating film. Part I. Theoretical model, *J. Lubrication Tech.* **92**, 451 (1970).
14. J. C. Coyne and H. G. Elrod, Conditions for the rupture of a lubricating film. Part II. New boundary conditions for Reynolds equation, *J. Lubrication Tech.* **93**, 156 (1971).
15. C. Fall, A theoretical model of striated film-rupture, *J. Lubrication Tech.* **104**, 165 (1982).
16. C. Fall, A theoretical model of striated film-rupture applied to the cylinder-plane, *J. Tribology* **107**, 419 (1985).
17. G. H. Golub and C. F. Van Loan, *Matrix Computations* (Johns Hopkins Press, Baltimore, 1989).
18. M. E. Gurfinkel Castillo and A. T. Patera, Three dimensional ribbing instability in symmetric forward roll film coating process, *J. Fluid Mech.* **335**, 323 (1997).
19. J. Greener, T. Sullivan, B. Turner, and S. Middleman, Ribbing instability of a two-roll coater: Newtonian fluids, *Chem. Eng. Comm.* **5**, 73 (1980).
20. S. F. Kistler and L. E. Scriven, Coating flows, in *Computational Analysis of Polymer Processing*, edited by J. R. A. Pearson and S. M. Richardson (Applied Science Publishers, London/New York, 1983), p. 243.
21. S. F. Kistler and L. E. Scriven, Coating flow theory by finite element and asymptotic analysis of the Navier–Stokes system, *Int. J. Numer. Methods Fluids* **4**, 207 (1984).
22. J. R. A. Pearson, The stability of uniform viscous flow under rollers and spreaders, *J. Fluid Mech.* **7**, 481 (1960).
23. E. Pitts and J. Greiller, The flow of thin liquid films between rollers, *J. Fluid Mech.* **11**, 33 (1961).
24. W. W. Pulkrabek and J. D. Munter, Knurl roll design for stable rotogravure coating, *Chem. Eng. Sci.* **38**, 1309 (1983).
25. K. J. Ruschak, A three-dimensional linear stability analysis for two-dimensional free boundary flows by the finite element method, *Comput. & Fluids* **11**(4), 391 (1983).
26. K. J. Ruschak, Coating flows, *Ann. Rev. Fluid Mech.* **17**, 65 (1985).
27. W. J. Silliman and L. E. Scriven, Separating flow near a static contact line: Slip at a wall and shape of a free surface, *J. Comput. Phys.* **34**, 287 (1980).
28. Y. Saad and M. H. Schultz, GMRES: A generalized minimal residue algorithm for solving nonsymmetric linear systems, *SIAM J. Sci. Stat. Comput.* **7**, 856 (1986).
29. Y. Saad, *Numerical Solution of Large Nonsymmetric Eigenvalue Problems*, RIACS Technical Report, NASA Ames Research Center, 88.39, 1988.
30. Y. Saad, Numerical methods for large eigenvalue problems, in *Algorithms and Architectures for Advanced Scientific Computing* (Manchester, Univ. Press, Manchester, 1994).
31. M. D. Savage, Cavitation in lubrication. Part 2. Analysis of wavy interfaces, *J. Fluid Mech.* **80**, 757 (1977).
32. M. D. Savage, Mathematical model for the onset of ribbing, *AIChE J.* **30**, 999 (1984).